NUMERICAL INVESTIGATION OF THE FLOW THROUGH A TRANSONIC TURBINE NGV WITH FILM COOLING

A PROJECT REPORT

Submitted in partial fulfillment for the award of the degree of

Bachelor of Technology
in
Mechanical Engineering

by

ROHIT SUNIL KANCHI - 19BME0188

School of Mechanical Engineering

Vellore Institute of Technology
(Deemed to be University under section 3 of UGC Act, 1956)

APRIL & 2023

DECLARATION BY THE CANDIDATE

I hereby declare that the project report entitled **"NUMERICAL INVESTIGATION OF THE FLOW THROUGH A TRANSONIC TURBINE NGV WITH FILM COOLING"** submitted by me to Vellore Institute of Technology University, Vellore in partial fulfillment of the requirement for the award of the degree of **Bachelor of Technology** in **Mechanical Engineering** is a record of bonafide project work carried out by me under the supervision of **Dr. Bibin John**. I declare that this report represents my concepts written in my own words and where others' ideas or words have been included, I have adequately cited and referenced the original sources. I further declare that I have adhered to all principles of academic honesty and integrity and have not misrepresented or fabricated or falsified any idea/data/fact/source in my submission. I understand that any violation of the above will be cause for disciplinary action by the Institute and can also evoke penal action from the sources which have thus not been properly cited or from whom proper permission has not been taken when needed. Further, I affirm that the contents of this report have not been submitted and will not be submitted either in part or in full, for the award of any other degree or diploma and the same is certified.

Place: Vellore Signature of the candidate

Date: 29/04/2023

VIT®
Vellore Institute of Technology
(Deemed to be University under section 3 of UGC Act, 1956)

School of Mechanical Engineering

BONAFIDE CERTIFICATE

This is to certify that the project report entitled **"NUMERICAL INVESTIGATION OF THE FLOW THROUGH A TRANSONIC TURBINE NGV WITH FILM COOLING"** submitted by **Rohit Sunil Kanchi (19BME0188)** to Vellore Institute of Technology University, Vellore, in partial fulfilment of the requirement for the award of the degree of **Bachelor of Technology** in **Mechanical Engineering** is a record of bona fide work carried out by him/her under my guidance. The project fulfils the requirements as per the regulations of this institute and in my opinion meets the necessary standards for submission. The contents of this report have not been submitted and will not be submitted either in part or in full, for the award of any other degree or diploma and the same is certified.

Project Guide **Head of the Department**

Internal Examiner **External Examiner**

ACKNOWLEDGEMENTS

I wish to express my profound gratitude to my esteemed mentor, Dr. Bibin John, for his invaluable guidance and assistance throughout the course of my project. His direction has paved the way for me to conduct further research with competence and proficiency. His insightful advice and support were instrumental in ensuring the timely completion of this project, producing comprehensible results with practical applications.

Furthermore, I extend my appreciation to the Dean of the School of Mechanical Engineering, Dr. K. Devendranath Ramkumar, and the Head of the Department of Manufacturing, School of Mechanical Engineering, Dr. C. Pandivelan, for providing me with the necessary facilities and guidance to successfully complete this project.

Place: Vellore (**Rohit Sunil Kanchi)**

Date: 29/04/2023

TABLE OF CONTENTS

	TECHNICAL AND MANUFACTURING READINESS LEVEL	
	COURSE OUTCOME	

EXECUTIVE SUMMARY

Gas turbines form a vital part of the power plants and jet propulsion systems. The exit enthalpy of the gases from the combustion chamber (CC) governs turbine work. Intuitively, higher enthalpy would result in a higher work output. However, the temperature withstanding capacityof turbine blades, especially the first stator row, limits the enthalpy of gas exiting the CC. As part of a standard industrial practice adopted widely for decades, film-cooled blades are employed to increase the turbine work output and maximize blade-life expectancy. The first objective of the current investigation is to numerically predict and validate the predictions of the aero-thermal aspects of the flow through a high-pressure transonic linear stator row. The second objective of the investigation is to predict the film-cooling effectiveness for the same blade geometry and study the effect of changing the hole shape on the film-cooling effectiveness. The baseline blade geometry for the aero-thermal investigation and film coolingstudies is the LS-89 blade, developed and tested at the Von-Karman Institute for Fluid Dynamics in their isentropic compression tube facility (CT-2). The original hole shape is circular whilst the modified hole is based on the 777-hole configuration widely adopted in theindustry. Two-dimensional results obtained from the Transition SST model are listed and compared with the k-w SST model's prediction in the aero-thermal studies. An excellent matchwas obtained with the experimental heat transfer and isentropic blade Mach number distributions in the aero-thermal study. An excellent match was obtained with the heat transferdistributions for the film-cooled cases as well. A comparison between the 777-hole and the circular shapedhole configurations revealed that the 777-hole provided better cooling performance on the pressure side. Over the suction side, the cooling from the 777-hole was found to be better thanthe circular hole for up to S = 39[mm], after which the heat transfer into the blade wall increased.

In conclusion, the methodology followed predicted the aero-thermal characteristics of the transonic and transitioning boundary layer flow through the chosen nozzle guide vane excellently and this methodology of increased prediction potential may serve as a test case forfuture studies in the same field. Finally, the investigation revealed the potential of the 777-hole's enhanced cooling performance.

Keywords: *Transonic Turbine; NGV; Film Cooling;*

LIST OF TABLES

LIST OF FIGURES

LIST OF SYMBOLS AND ABBREVIATIONS

Re:	Reynold's Number
M:	Mach Number
C:	Chord Length
S:	Blade Length
γ:	Specific Heat Ratio
k:	Thermal Conductivity
C_p:	Specific Heat Capacity
R:	Universal Gas Constant
T:	Temperature
ρ:	Density
μ:	Dynamic Viscosity
P:	Pressure
h:	Heat Transfer Coefficient
q:	Heat Flux
Tu:	Turbulence Intensity
BR:	Blowing Ratio $\rho_c.u_c/\rho_\infty.u_\infty$
u:	Velocity
$\overline{Variable}$	Time averaged Variable
x	X direction in Cartesian System
y	Y direction in Cartesian System
μ_t	Turbulent Viscosity
η	Turbulent Viscosity Ratio
V	Velocity magnitude
u	X velocity
v	Y velocity
w	Z velocity
Cax	Length in axial direction from LE
is	Isentropic
o	Total Variable
w	Wall
∞	Freestream Variable

c	Coolant Variable
Turb	Turbulence
SS	Suction Side
PS	Pressure Side
CC	Combustion Chamber
SST	Shear Stress Transport
TKE	Turbulence Kinetic Energy
BC	Boundary Condition
CFD	Computational Fluid Dynamics
LE	Leading Edge
TE	Trailing Edge
BR	Blowing Ratio
VKI	Von Karman Institute for Fluid Dynamics
NGV	Nozzle Guide Vane
LES	Large Eddy Simulation
RANS	Reynold's Averaged Navier Stokes

CHAPTER 1

INTRODUCTION AND LITERATURE REVIEW

Gas turbines form a vital part of power plants and jet propulsion. The exit enthalpy of gases from the combustion chamber (CC) governs turbine work. Higher enthalpy would result in higher work output. However, temperature withstanding limits of turbine blades limit the amount of heat released in the CC. The first set of nozzle guide vanes (NGV) is the highest temperature affected zone. The current investigation includes numerical studies of the aero-thermal aspects of flow inside NGV with and without film cooling.

In the aero-thermal study of the flow field, experimental data was available and has been used to validate the numerical methodology employed in the current study. The test case is called LS-89, which is a nozzle guide blade geometry designed and tested for a high-pressure turbine at the Von Karman Institute for Fluid Dynamics. This blade was later employed in an extensive film cooling experimental study by Fontaneto et al (Studi et al., 2014). Challenges in the numerical prediction of heat transfer into the blade arose from the very nature of the flow field itself, which was transonic and had a transitioning boundary layer on the suction and pressure sides of the blade.

The aero-thermal investigation of the NGV blade performed at VKI by Arts et al (Arts et al., 1990) consisted of several experiments, namely Blade Isentropic Mach number distribution, flow periodicity checks, turbulence characterization and heat transfer coefficient measurements. The Mach number, turbulence characterization and heat transfer measurements were taken as test cases to validate the numerical data and methodology. The film cooling studies performed by Fontaneto et al. (Studi et al., 2014) on the LS89 blade involved turbulence characterization, heat transfer studies with film cooling at different blowing ratios and without film cooling at various Mach and Reynold's number combinations and finally, the blade efficiency characterization.

The experiments were originally performed to serve as test cases for the different numerical models developed over the years to predict turbulent flows, such as the LES and RANS models and hybrid LES-RANS model (Asiegbu et al., 2022). The numerical predictions of the film cooling experimental data obtained from literature based on the current blade under review have been rather poor in the error percentage in terms of deviations of the CFD predictions from the experimental data. The current study aimed at establishing a framework to numerically solve and predict the experimental data well. This framework was validated and

was followed to modify the film cooling holes geometry on the same blade and compare the flow physics and its effects on the efficiency of the cooling system with the former film cooled case and non-cooled case. An excellent match with the experimental data was observed for both the film-cooled and non-cooled cases in the current study.

Extensive research has been performed in the aero-thermal aspects of the fluid flow through different types of nozzle guide vanes. High Pressure and Transonic guide vanes are very popular test cases for validating CFD codes. The current investigation uses (Arts et al., 1990) as a baseline study for the aero-thermal investigation studies and (Studi et al., 2014) as a baseline study for the film cooling parametric studies. The NGV blade called LS89 was investigated for its aero-thermal aspects by Arts et al. (Arts et al., 1990) by performing experimental studies and obtaining the blade velocity and heat transfer distributions. The heat transfer distributions were extensively investigated in which the effects of Freestream Turbulence, exit isentropic Mach number and Reynold's number were studied. Higher turbulence intensities showed greater heat transfer only at adversely high Reynold's numbers and Mach numbers. Generally, the suction side and pressure side boundary layers remained in a transitional state.

The LS89 blade was investigated by Fontaneto et al. (Studi et al., 2014) for the aero-thermal aspects in film cooling for the said blade. For the suction side, investigations revealed that at high Reynold's number (1.5e+06) and moderate exit Mach number (0.8) the cooling effectiveness increased with increasing blowing ratio up to a certain limit (0.4 – 0.9). For an exit Mach number of 1.1, the trend is similar to the previous case of M = 0.8 but post a shock on the suction side, this trend changes and becomes erratic. For the pressure side, at M = 0.8 and M = 1.1, similar trends are followed in which the film cooling effectiveness decreases rapidly for higher blowing ratios near the region of the exit of cooling holes, but reverses in the behavior as the fluid flows downstream of the blade.

The above two experimental investigations have served as test cases for many CFD analysts and researchers. Broadly speaking, researchers in this particular field of numerical studies have two agendas. One is to validate a new CFD approach or model with the experimental data and two is to better understand the flow physics through the nozzle guide vane. Hadi Yavari et al. (Yavari et al., 2019) investigated the flow through a high pressure NGV and redesigned the blade to increase its efficiency. 22% lower coolant consumption was achieved and the metal

temperature reduced significantly too. Phan et al. (Phan et al., 2020) investigated the effects of inflow conditions on the LS89 blade. The methodology was validated well with the experimental data from Arts et al. (Arts et al., 1990).

In the studies performed, the inlet turbulence was found to rapidly decay from the inlet to the leading edge of the blade. A comparison between the steady state and time averaged unsteady NS calculations revealed no significant differences in the computations. The turbulence models employed were k-w SST, Transition SST and laminar model. A comparison was made between the models and the Transition SST predicted the experimental data best. Collado et al. (Collado, 2018) studies the differences between Laminar, steady RANS, unsteady RANS and complete LES turbulence models when attempting to predict the experimental data on the LS89 blade from Arts et al. [1]. The LES model gave best results as compared to its RANS counterparts. Torreguitart el al. (Torreguitart et al., 2018) redesigned the LS 89 blade and found that the pressure loss could be reduced by up to 16 %. However, there is a lack of experimental evidence for this.

Bassi et al. (Bassi et al., 2016) numerically investigated and attempted to validate the high-order discontinuous Galerkin RANS solver with the experimental data on film cooling performed on the LS89 blade by Fontaneto et al. (Studi et al., 2014). It was found that the k-w model fails to reproduce any laminarization of the boundary layer over the suction side and over predicts the heat transfer. The Galerkin computations did predict the data better, although not satisfactorily. In a similar attempt to predict the film cooling heat transfer distribution and film cooling effectiveness on the LS89 blade numerically and test the turbulence models RANS and hybrid RANS, Asiegbu et al. (Asiegbu et al., 2022) made a comparison between a scale resolving hybrid model [SRH] and RANS model and the latter [Transition-SST] predicted the film cooling better. However, a satisfactory match with the experimental film cooled blade heat transfer distribution data was not observed.

Various important parameters affect the film cooling performance. Coolant and mainstream flow factors such as mass flux ratio, density ratio, momentum ratio, turbulence, hole geometry and configuration and the airfoil geometry affect film cooling effectiveness. Under hole geometry, certain holes with shapes such as rectangular and fan-shaped provide better spread of the coolant as compared to cylindrical holes. The shaped holes also prevent jet separation and higher turbulence intensities near the cooling holes, thus allowing higher blowing ratios.

Location wise for an NGV blade, in addition to the suction side and pressure side cooling, leading edge and trailing cooling are also performed to better cool the blades. Leading edge cooling is often referred to as "shower-head cooling" (Bogard, 2006; Dyson et al., 2013; Dees et al., 2012).

Thole et al (Schroeder et al., 2014) developed the 777-hole shape which was found to have higher film-cooling effectiveness and better coolant spread due to its shape. It is known to have been employed in various industrial turbines due to its improved cooling performance. Better spread of the coolant aids in increasing the pitch of the holes and hence in turn reducing the number of holes. This is significant when the structural integrity of the blade is in question. The 777-hole shape has been used in the investigation and its performance has been compared with the former cooled cases. For the same coolant and freestream flow conditions, the 777-hole configuration resulted in a better cooling performance on the pressure side and a rather poor performance on the suction side due to increase in the turbulence within the boundary layer. The spread of the coolant however, was found to be much better in the case of the 777-hole in contrast to its circular counterpart.

It has been understood from the current literature that the numerical prediction of heat transfer and turbulence characteristics in transitional boundary layer and transonic wall bounded flows is a challenge, especially when RANS Turbulence models are employed. Moreover, film cooling studies for transitional flows are not often reported in the literature. Most of the reported film cooling studies were carried out using unstructured mesh due to the very complex nature of the computational domain. Use of such less accurate mesh elements noted to be resulting in underprediction/overprediction of heat transfer coefficient and film cooling effectiveness when comparing with experimental measurements. Therefore, there is a scope for carrying out computational analysis of NGV cascade aerodynamics and film cooling studies by using a much accurate, systematic numerical framework. There was hence, value in performing parametric studies on the shape of film cooling holes using the above said framework of improved prediction potential.

The organisation of the manuscript is as follows. In section 2, the experimental methodology, computational domain geometries and the computational grid methodology has been discussed. In section 3, the boundary conditions and flowing fluid (air) properties chosen have been laid down. In section 4, the solution methodology has been discussed in depth, which involves the

turbulence model, numerical methodology and solver methods employed in the numerical studies. The flow variable measurement techniques have been discussed in section 4 as well. The section 5 gives the results and discussion for the cooled and non-cooled cases with a comparison between the circular hole shape and 777-hole shape cooling holes. Finally, the section 6 lays down the concluding remarks.

CHAPTER 2
METHODOLOGY AND EXPERIMENTAL WORK

2.1 Experimental work and numerical grids

The LS89 blade geometry was developed at the Von Karman Institute for Fluid Dynamics (VKI) and tested in their native compression tube (CT-2) facility (Fig. 2.1) for a wide range of exit Reynold's and Mach numbers. The experimental investigation was performed by (Arts et al., 1990) and this experiment has served as a test case for many CFD engineers for decades. More about the exact experimental techniques and test case description can be found in (Arts et al., 1990). The main blade geometrical dimensions are given in Table 2.1 and the corresponding geometry is shown in Fig. 2.1.

The base-line geometry adapted for the present numerical study is the VKI test case blade (Arts et al., 1990), which had the following experimental components:

a. Turbulence Characterization using Hot Wire Probe.
b. Flow Periodicity Checks: Using downstream static pressure taps.
c. Blade Velocity (Mach Number) Distributions: Using Pressure taps and isentropic flow relations to compute the Mach number.
d. Schlieren Flow Visuals.
e. Blade Convective Heat Transfer Coefficient Measurements: Using thin Platinum foils painted onto the blade.

The tests listed above were performed on a blade, which was the central blade of a group of five blades in a linear cascade arrangement mounted inside the CT-2 test chamber section. The test section is part of a larger experimental apparatus known as the compression tube facility or CT-2 at VKI.

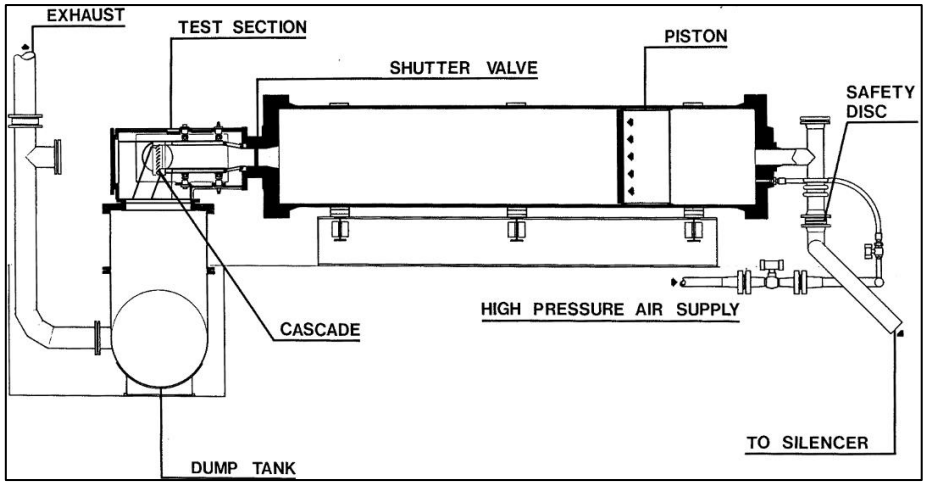

Fig 2.1. Compression Tube Facility at VKI for Fluid Dynamics.

Image courtesy Arts et al (Arts et al., 1990).

The cooling tests performed by Fontaneto et al (Studi et al., 2014) were composed of two rows of staggered holes on each side of the blade just downstream of the leading edge. These were fed separately by two separate feeding chambers. The two rows on the suction side and the first one of the pressure side are inclined of 35^o with respect to the local surface tangent while the second row of the pressure side is parallel to the latter. Each hole is 0.5 [mm] in diameter with a pitch of 1.5 [mm], hence making the staggering pitch 0.75 [mm]. The relevant geometry is shown in Fig. 2.3.

Table. 2.1. Geometrical parameters for the LS-89 blade

Parameter	**Value**
C	67.647 [mm]
C_{ax}	36.985 [mm]
γ	55^o
o	14.93 [mm]
g	57.5 [mm]
H	100 [mm]
r_{TE}	4.13 [mm]

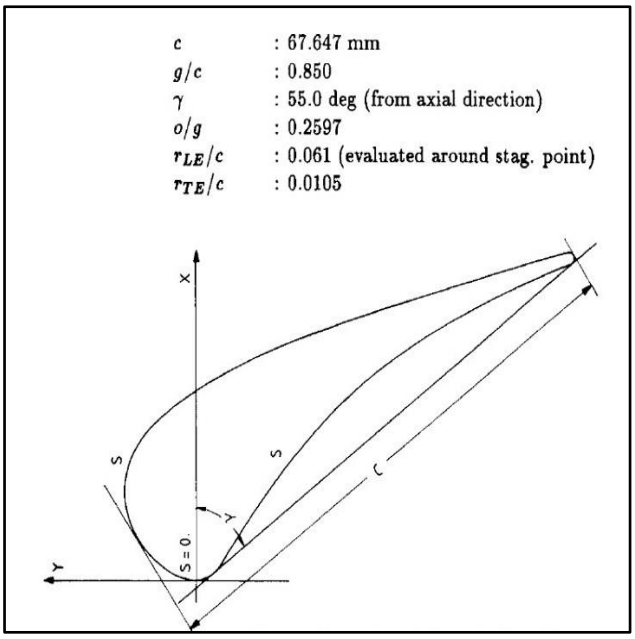

Fig 2.2. The LS89 blade. Image courtesy Arts et al (Arts et al., 1990)

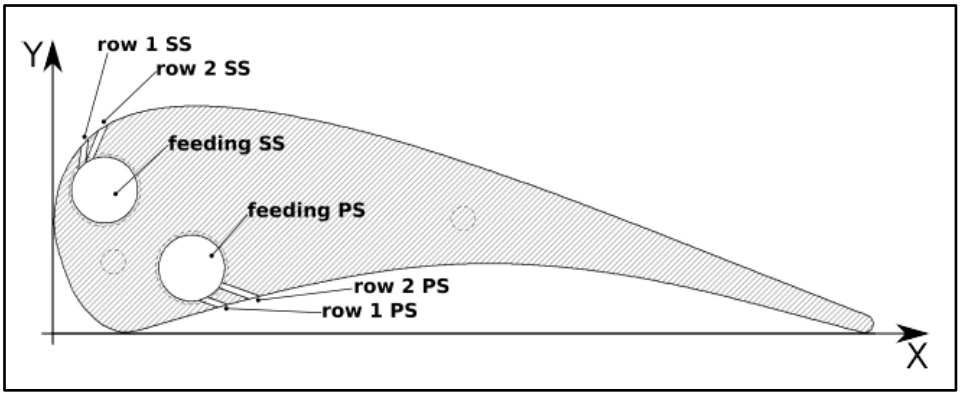

Fig 2.3. Cooling configuration in the cross-sectional view.

Image courtesy Fontaneto et al (Studi et al., 2014)

With reference to the experimental components aforementioned (a-c), the experimental dataset for (c) consists of two tests and the dataset for (e) consists of seven tests with different turbulence intensities and exit Mach and Re numbers to study the effect of those parameters on the flow physics. The current study validates the numerical methodology using the list of experiments in Tables. 2.2 and 2.3. It should be noted that these tests will be referred to with their respective test numbers here onwards.

Table 2.2. List of experiments chosen for the numerical aero-thermal study

Test Case Number	**Test Type**	**Exit Re**	**Exit Mach**	**Inlet Turbulence Intensity**
1	Blade Heat Transfer Coefficient Distribution	5e+05	0.92	1%
2	Blade Mach Number Distribution	1e+06	0.875	1%
3	Blade Mach Number Distribution	1e+06	1.02	1%

Table 2.3. List of experimental test cases for the film cooling study

Test Case Number	**Test Type**	**Exit Re**	**Exit Mach**	**BR**	**Inlet Turbulence Intensity**
4	Suction Side Cooling	1.5e+06	0.8	0.55	5.3%
5	Pressure Side Cooling	1.5e+06	0.8	1.53	5.3%

Given the flow periodicity which is evident from Fig. 2.4. below, the flow domain was modelled with periodic boundaries as shown in Fig. 2.5. The Fig. 2.4. represents an isentropic Mach number distribution in the exit plane which was 16 [mm] downstream of the trailing edge plane.

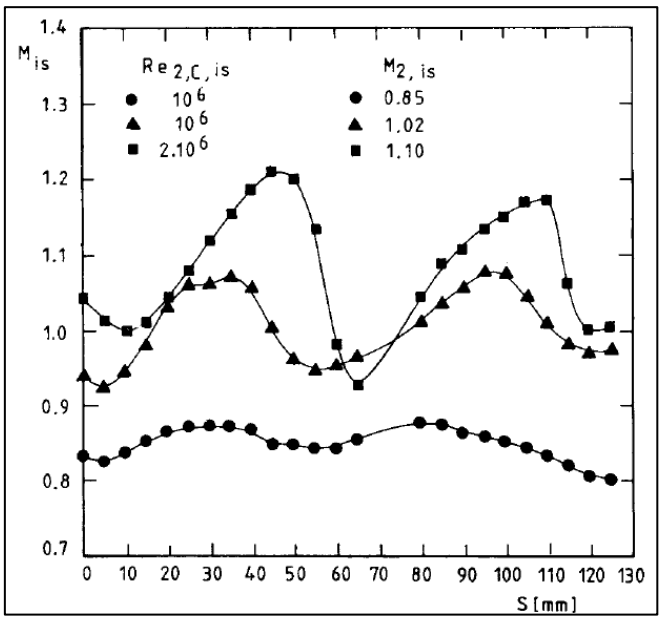

Fig 2.4. Downstream periodicity measurements.

Image courtesy Arts et al (Arts et al., 1990)

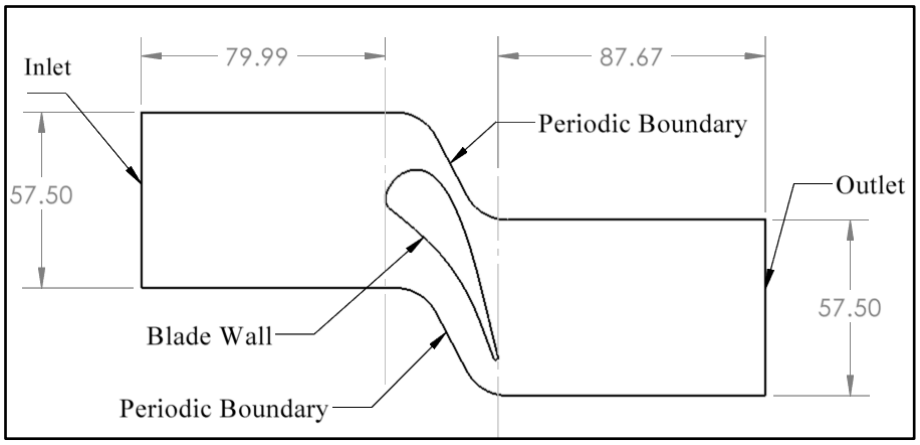

Fig 2.5. Computational domain for the non-cooled cascade

The flow domain is in 2D because the measurements were taken along the mid-span of the central blade of the linear cascade and this was situated in the clean flow region, away from the end-walls. The measurements portray a span-wise averaged behavior. The mesh was made

to be completely structured and a mesh convergence study was performed during the simulations. An image of the mesh which gave a mesh independent solution with 61,175 elements is shown below in Fig. 2.6.

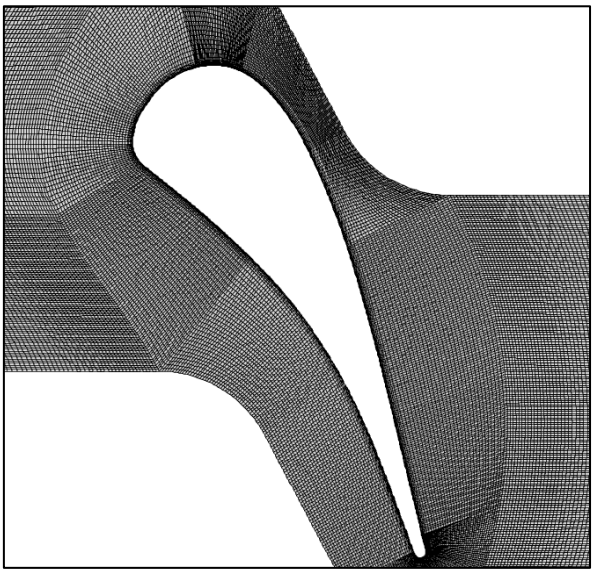

Fig 2.6. Structured computational grid for the non-cooled case.

The mesh was tailored to the flow field to best predict the convective heat transfer and Mach number measurements. A structured O-gride enclave was made around the blade and this O-grid which involves the boundary layer mesh ensured a y+ of less than 1 around the blade to aid the turbulence model in better capturing the boundary layer effects. This was essential because the Transition SST model was used and this RANS based model requires that the y+ value be less than 1 to model capture the boundary layer effects better. The minimum and maximum orthogonal quality was found to be 0.481 and 0.973 respectively. The minimum and maximum skewness values were 0 and 0.673 respectively. The overall mesh quality based on the metrics specified was observed to be of good quality. This was further validated when the experimental data matched well with the numerical prediction.

The computational domain for the film-cooled case is shown in Fig. 2.7. Since the fluid domain was of a linear cascade with staggered rows, periodicity was given to a section cut from the entire domain in the spanwise direction as the measurements were taken in the clean flow region during the experiment. The plenum was not modelled in the computational domain. Fig. 2.8 shows the domain with periodicity applied in the span-wise direction. This led to two half-

holes on the periodic faces and one full hole in between in a staggered manner. The location of the cooling holes and injection angles can be found in Fontaneto et al (Studi et al., 2014).

A structured grid was generated for the given film-cooling geometry which can be seen in Fig. 2.9. An O-grid type mesh was generated for the cooling holes with boundary layer meshing for the walls of the holes (Fig. 2.10). Two separate grids were generated for the suction and pressure sides respectively. This was because two different turbulence models were used for each case. The Transition SST model under predicted the heat transfer for the pressure side cooling case, whilst the k-w SST model predicted the heat transfer distribution best. This was not the case for the suction side where a transitioning boundary layer was observed.

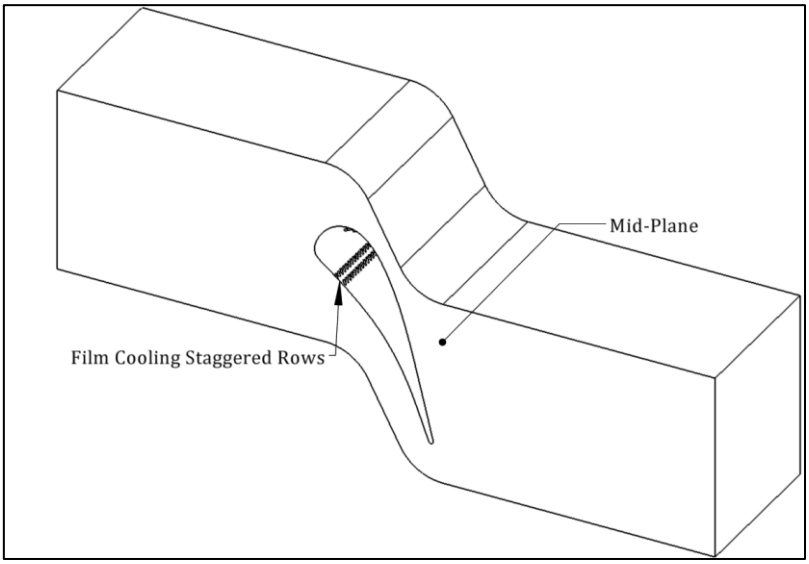

Fig 2.7. Film cooling computational domain

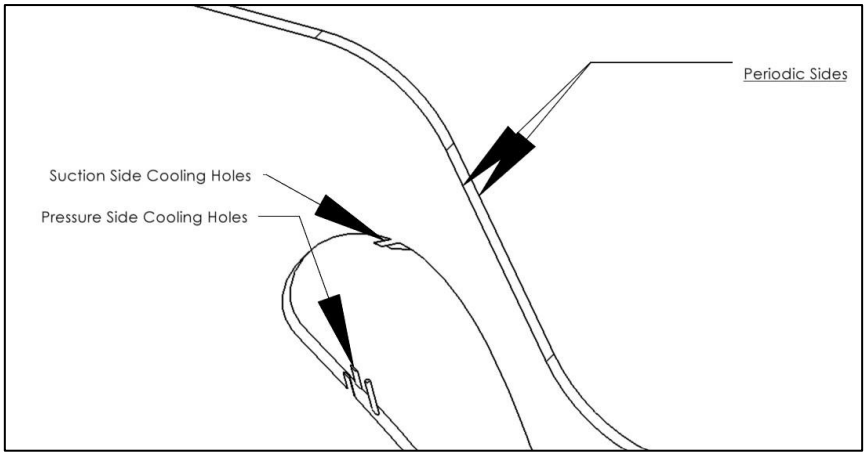

Fig 2.8. Film cooling computational domain with periodicity applied in the spanwise direction

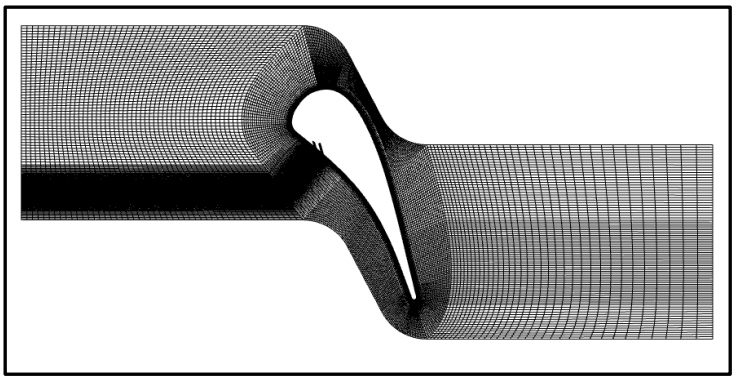

Fig 2.9. Pressure side cooling case computational grid (structured)

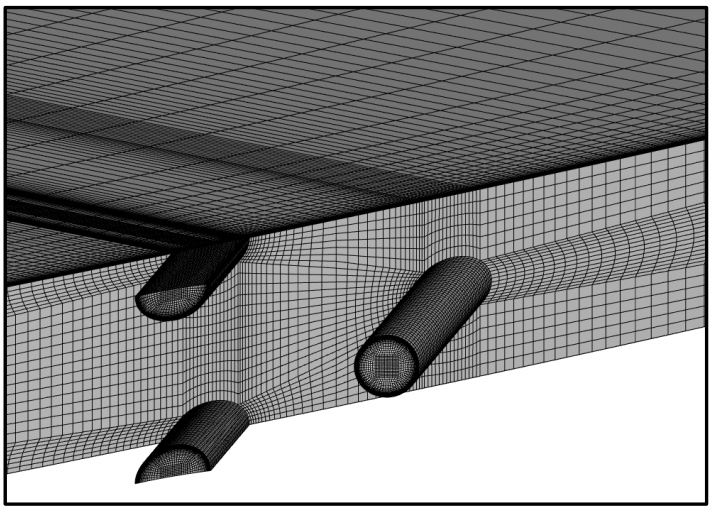

Fig 2.10 Structured O-grid shown for the cooling holes.

The minimum and maximum orthogonal quality were found to be 0.481 and 0.973 respectively. The minimum and maximum skewness values were 0 and 0.673 respectively. The overall mesh quality for the circular hole film-cooled blade grid based on the metrics specified was observed to be of good quality. It can be observed that the plenum was not modelled in this numerical investigation. This reduced the overall computational effort manifold.

The computational domain for the 777 hole is shown in Fig. 2.11. This domain was also discretized using structured grid generation techniques. A structured grid image is shown in Fig. 2.12. This was made separately for each side of the blade to compare with the cooled cases.

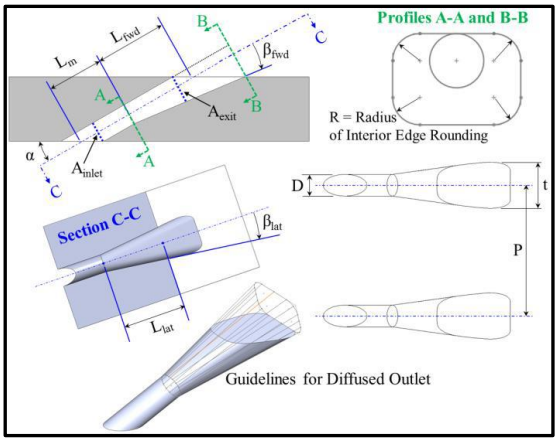

Fig 2.11. 777-hole fluid domain and hole shape. Image courtesy (Schroeder et al., 2014)

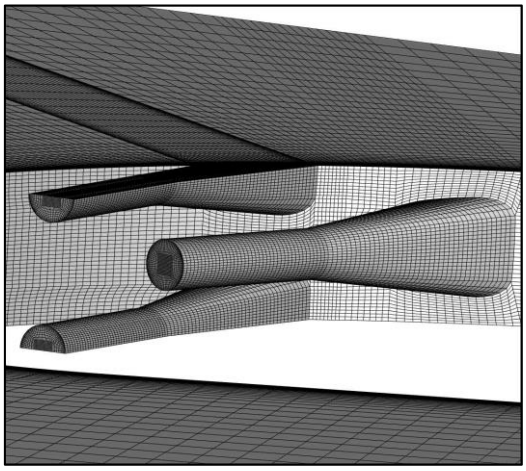

Fig 2.12. Structured grid of the 777-hole

The minimum and maximum orthogonal quality were found to be 0.481 and 0.973 respectively. The minimum and maximum skewness values were 0 and 0.673 respectively. The overall mesh quality for the circular hole film-cooled blade grid based on the metrics specified was observed to be of good quality.

2.2 Boundary conditions and flowing medium properties

The inlet and outlet in all the simulations performed were given to be of Pressure inlet and Pressure outlet respectively. All walls were given the No-Slip BC. All periodic boundaries were given translational periodicity. All the coolant hole inlets were given a velocity inlet BC with the static temperature specified. Detailed information on the boundary conditions can be seen in the Fig 2.13.

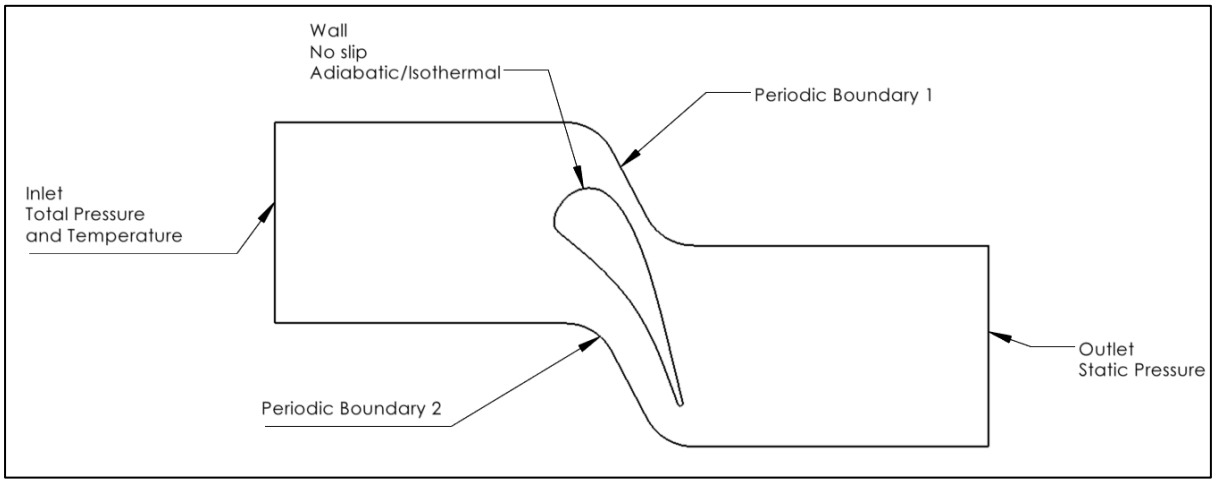

Fig 2.13. Boundary conditions for the computational domain

It must be noted that the isothermal BC was applied to the walls because the testing time was about 500ms and hence the initial wall temperature was given in an isothermal BC in a steady state analysis. The outlet pressure was set to approximately 0.98 times the exit pressure measured experimentally. The inlet to the tubes was given as a velocity inlet. The velocity was calculated based on isentropic flow relations from the BR, DR and pressure ratios measured in the experiment (Studi et al., 2014).

Air is the flowing fluid medium and this has been numerically modelled as an ideal gas. The thermal conductivity is based on the kinetic theory for ideal gases modelled with the Lennard-Jones Potential theory. The specific heat Cp has been modelled using a piece-wise polynomial in Fluent, which gives the C_p as a function of temperature. The dynamic viscosity has been given using the popular Sutherland correlation for ideal gases.

2.3 Turbulence modelling

ANSYS Fluent was used as the CFD code to predict the experimental data. Fluent works on the Finite Volume Method. The domain is discretized into several small control volumes and the conservation of mass, momentum and energy is then applied to these volumes and the fluid

flow equations are numerically solved. The flow being of a turbulent nature, required a numerical model which could predict the turbulent nature of the flow field. In order to capture this well, the Reynold's Averaging Navier Stokes or RANS equations were developed by Osborne Reynold by splitting the flow variables into constant and fluctuating (temporally and spatially) components. The equations are closed using various turbulence models, each with their different predictive capabilities. These equations for compressible viscous flows are given in equns 1-5. The continuity equation is given in equn 1. The Reynolds equations are given in equns 2-4 and the scalar transport equation is given in equn 5.

$$\frac{\partial \bar{\rho}}{\partial t} + div(\bar{\rho}\widetilde{\boldsymbol{U}}) = 0 \dots (1)$$

$$\frac{\partial(\bar{\rho}\widetilde{U})}{\partial t} + div(\bar{\rho}\tilde{U}\widetilde{\boldsymbol{U}}) = -\frac{\partial \bar{P}}{\partial x} + div(\mu \text{grad}\tilde{U}) + \left[-\frac{\partial\overline{(\bar{\rho}u'^2)}}{\partial x} - \frac{\partial\overline{(\bar{\rho}u'v')}}{\partial y} - \frac{\partial\overline{(\bar{\rho}u'w')}}{\partial z}\right] + S_{Mx} \dots (2)$$

$$\frac{\partial(\bar{\rho}\widetilde{V})}{\partial t} + div(\bar{\rho}\tilde{V}\widetilde{\boldsymbol{U}}) = -\frac{\partial \bar{P}}{\partial y} + div(\mu \text{grad}\tilde{V}) + \left[-\frac{\partial\overline{(\bar{\rho}u'v')}}{\partial x} - \frac{\partial\overline{(\bar{\rho}v'^2)}}{\partial y} - \frac{\partial\overline{(\bar{\rho}v'^{w'})}}{\partial z}\right] + S_{My} \dots (3)$$

$$\frac{\partial(\bar{\rho}\widetilde{W})}{\partial t} + div(\bar{\rho}\tilde{W}\widetilde{\boldsymbol{U}}) = -\frac{\partial \bar{P}}{\partial z} + div(\mu \text{grad}\tilde{W}) + \left[-\frac{\partial\overline{(\bar{\rho}u'w')}}{\partial x} - \frac{\partial\overline{(\bar{\rho}w'v')}}{\partial y} - \frac{\partial\overline{(\bar{\rho}w'^2)}}{\partial z}\right] + S_{Mx} \dots (4)$$

$$\frac{\partial(\bar{\rho}\widetilde{\phi})}{\partial t} + div(\bar{\rho}\tilde{\phi}\widetilde{\boldsymbol{U}}) = div(\Gamma_{\phi} grad\tilde{\phi}) + \left[-\frac{\partial\overline{(\bar{\rho}u'\phi')}}{\partial x} - \frac{\partial\overline{(\bar{\rho}v'\phi')}}{\partial y} - \frac{\partial\overline{(\bar{\rho}w'\phi')}}{\partial z}\right] + S_{\phi} \dots (5)$$

For the flow field under study, the k-w Shear Stress Transport and the Transition SST models were employed to better predict the turbulence characteristics of the flow. The Transition SST model is a modified version of the k-w SST model and is used to predict flows with boundary layers at wall transitioning from laminar to turbulent. The model is available as a part of the Fluent package. The specifics of both the models can be found in the ANSYS Theory Guide.

2.4 Grid independence studies

The approach followed during convergence study was to initially obtain a first order accurate solution with scaled residuals of energy, momentum, continuity and turbulence model variables

below 1e-06 and then switch to second order discretization scheme and solve the equations again. This approach ensured smooth convergence. As for the mesh independency, three meshes for each simulation component were made with increasing number of elements. The second mesh had twice as many elements as the first, and the same was for the third and second meshes.

It was found in all the simulations that the second and third mesh produced results with negligible differences and hence the second mesh was used for further studies in the same type of simulation mode, i.e., non-cooled/film-cooled. It was ensured that refinement to the grid was made in regions of interest, such as the wall, the film cooling holes and the leading edge of the blade, which demanded a sufficient number of elements to resolve the flow field in that region.

The details pertaining to the grid such as number of elements, mesh quality and images of the grids for each case, i.e., the non-cooled and cooled cases have already been shown and discussed in Sec. 2. The study has in total five grids. The 1st grid is for the non-cooled case validation study, the 2nd and 3rd are for the suction side and pressure side cooling validation studies, and finally the 4th and 5th grids are for the 777-hole shaped cooling hole simulations for the pressure and suction sides respectively, for the comparison study. All these grids are the grids which gave a mesh independent solution.

2.5 Numerical solution methods

ANSYS Fluent was used as the CFD code to predict the experimental data. Fluent works on the Finite Volume Method. The domain is discretized into several small control volumes and the conservation of mass, momentum and energy is then applied to these volumes and the fluid flow equations are numerically solved. Under the solver methods, the Density Based NS Solver was employed. With an implicit formulation the AUSM flux scheme with least squares cell based gradient discretization scheme was used. The spatial discretization schemes for all the flow variables were initially of first order accuracy.

The residuals generally varied for the first order accurate solution from 1e-03 to 1e-06 with continuity residuals being around 1e-03. This was the scaled residual. Post switching to second order, the residuals were normalized and this gave a residual range of up to 1e-04 to 1e-07. The integrated quantities such as heat transfer and skin friction were monitored during convergence. The global energy and mass imbalances were monitored as well. The imbalances at the end of

the iterations were made sure to be negligible. Finally, the post-processing was done using ANSYS CFD Post for the pressure and heat transfer measurements, and the contour plots. The graph plots were obtained from MATLAB and the mesh images and shadowgraphs were obtained from TECPLOT 360.

2.6 Flow variable measurement and characterization

The flow variables include the turbulence, thermodynamic and integrated quantities such has heat flux, turbulence intensity, temperature, pressure, etc. These quantities were characterized and measured in the experimental setup using techniques such as hot wire anemometry, pressure gauges, platinum thin foils, etc. The measurement of flow variables was hence important to be carefully measured correctly and characterized before comparison of results with the experimental data. The methodology is given below.

1. Inlet Turbulence Parameters:

   The inlet turbulence was characterized by two variables, namely the turbulence intensity and turbulence viscosity ratio. These were crucial to be correct since the Transition-SST model when employed leads to a very steep turbulence decay in the freestream. This decay can be predicted using an analytical solution which is given in the ANSYS Guide. A graph of the turbulence decay as an example is shown in Fig. 2.14. Turbulence intensity was defined as given in the equn. 6, and the turbulent viscosity ratio was defined as given in equn. 7. The analytical equation predicting the turbulence intensity at a location downstream of the inlet is given in the equn. 8.

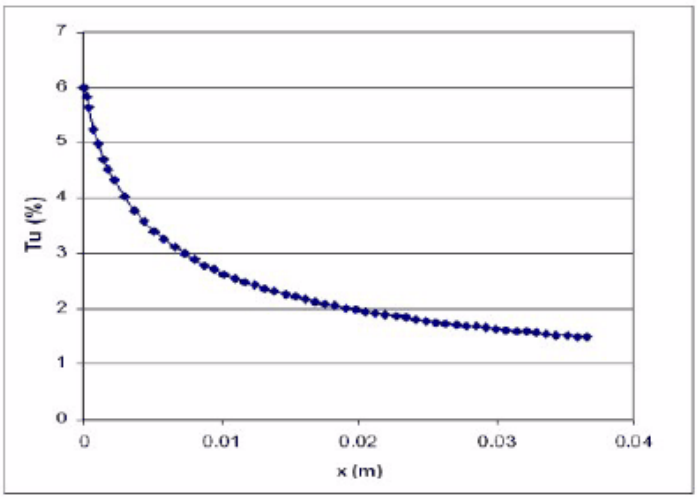

Fig 2.14. Turbulence decay in the freestream.

$$Tu_{\infty} = \frac{\sqrt{\overline{u'^2}}}{\bar{u}} \ldots (6)$$

$$\eta_{turb} = \frac{\mu_{turb}}{\mu} \ldots (7)$$

$$Tu_{\infty,x} = \left(Tu_{inlet}{}^2 \left[1 + \frac{3\rho V x \beta Tu_{inlet}{}^2}{2\mu\eta_{turb}} \right]^{\frac{-\beta^*}{\beta}} \right)^{0.5} \ldots (8)$$

Where,

- x is the distance from the inlet of the domain in the free stream.
- β=0.09 and β^*=0.0828

The turbulence intensity and turbulent viscosity ratio were therefore changed at the inlet so as to acquire the required turbulence intensity at the leading edge. A higher turbulent viscosity ratio was required to be kept in order to reduce the decay rate of the turbulence intensity in the freestream.

2. Exit Mach and Reynold's numbers:

The exit Mach number was taken as the average of the Mach number distribution along the y axis direction in the exit plane which was parallel to and 16mm downstream of the trailing edge plane. The Re number was characterized by the total inlet pressure and exit static pressure in the experiment. For the same exit Mach number, inlet total temperature and different total pressures, a wide range of exit Re numbers can be obtained. The Re number was length based and the characteristic length for the Reynold's number was taken to be the chord length of the airfoil, as was done in the experiment.

The exit Mach number was obtained from equn. 9.

$$M_{2is} = \frac{V_2}{\sqrt{\gamma . \mathrm{R} . \mathrm{T}_2}} \ldots (9)$$

The exit isentropic Reynold's number was calculated using the equn. 10.

$$Re_{2,is} = \frac{\rho_2 . V_2 . \mathrm{L}}{\mu_2} \ldots (10)$$

Where μ_2 is the dynamic viscosity in the exit plane based on the average temperature using Sutherand's law in the exit plane obtained from the equation. 3, V_2 is the average exit velocity and ρ_2 is the exit averaged density obtained from the ideal gas law in equn.12. P_2 in the equn. 12 can be found out using equn. 13 by replacing M with M_{2is}.

$$\frac{T_o}{T_2} = \left(1 + \left(\frac{\gamma - 1}{2}\right) {M_{2is}}^2\right) \ldots (11)$$

$$\rho_2 = \frac{P_2}{R\mathrm{T}_2} \ldots (12)$$

The boundary conditions were given to the flow domain based on experimental data given in the Technical Note 174 (n.d.), a supporting document to the experimental paper by Arts et al (Arts et al., 1990).

3. Blade Mach number measurements:

   The blade Mach number M_{is} distribution was obtained using isentropic flow relations between pressure ratio and Mach number. This was done in the experimental setup as well. The reason for doing this is that at the wall, the boundary layer effects come into the picture and the velocity at wall is zero, which is the no slip boundary condition. M_{is} was thus obtained using the equn. 13.

$$\frac{P_o}{P_w} = \left(1 + \left(\frac{\gamma - 1}{2}\right) {M_{is}}^2\right)^{\frac{\gamma}{\gamma - 1}} \ldots (13)$$

4. Blade Heat Transfer Measurements:

   Heat transfer measurements were taken by obtaining the heat flux along the blade at different locations and obtaining the heat transfer coefficient h using the method followed in (Arts et al., 1990). The equn. 14. gives the formula used to calculate h.

$$h = \frac{q}{T_o - T_w} \ldots (14)$$

CHAPTER 3
RESULTS AND DISCUSSION

The results and discussion part of this manuscript has been subdivided into mainly 3 parts

a. Non-cooled case
b. Pressure side and suction side cooling (Circular Hole)
c. Comparative study between the 777 hole and circular hole shapes

3.1 Non-Cooled case

As aforementioned in this manuscript, to avoid repetition and lengthiness the test cases are referenced using their corresponding numbers as given in chapter 2.

The heat transfer measurements were performed numerically and the mesh independency study was based on these measurements. Finally, the mesh which gave a mesh independent solution was used for the blade isentropic Mach number distributions.

Test case 1

The boundary conditions for the test case 1 are presented in the table 3.1.

Table 3.1. BC for the test case 1

Inlet	Total Pressure: 90400 Pa Total Temperature: 404.1 K Freestream Intermittency: 1 Turbulent Intensity: 1.3% Turbulent Viscosity Ratio: 10
Outlet	Static Pressure: 51620 Pa
Walls	No Slip BC Temperature: Isothermal BC, 301.65K
Periodicity	Conformal Translational Periodicity
Reference Pressure	0 Pa

The mesh independency study results are shown below in Figs. (3.1 & 3.2) for the suction and pressure sides respectively. The comparison of numerical prediction with the experimental data is shown in the Figs. (3.4 & 3.5) for the suction and pressure sides respectively. The heat

transfer rate sees a steep decrease in the value from the leading edge towards the trailing edge. However, the heat transfer near the leading edge is on the higher side because the freestream static temperature near the leading edge increases due to the stagnating effects of the blade leading edge on the flow. However, the freestream turbulence is relatively low at the leading edge. After the air flows downstream of the leading edge, the boundary layer starts to develop on each side of the blade. The flow conditions and its effects on the boundary layer decides the heat transfer rate as this value is in direct proportion to the convection at the wall and hence the turbulence intensity.

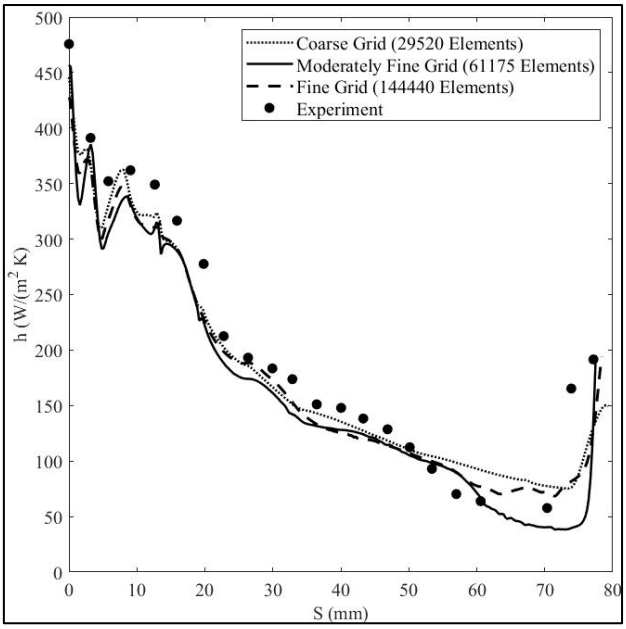

Fig 3.1. Mesh independency results for the suction side Test Case 1

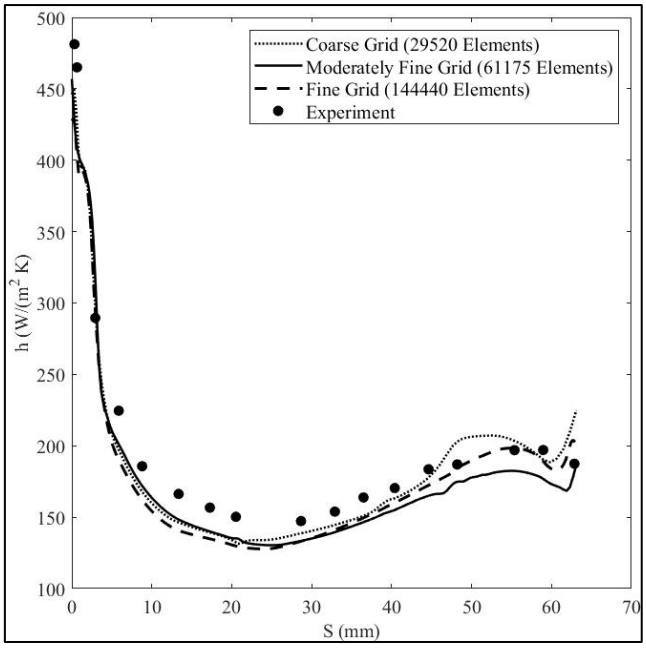

Fig 3.2. Mesh independency results for the pressure side Test Case 1

Air tends to achieve stagnation conditions when it encounters the leading edge. The static temperature rises towards the total value and the difference in temperature between the air and blade wall then increases. However, since air is in motion, there is convection as well due to the freestream turbulence already present in the flow. It is therefore necessary to understand the contributions of each, i.e., the stagnating of the fluid and the turbulence intensity and hence higher forced convection in increasing the htc in different regions of the blade, especially the leading and trailing edges.

The turbulence intensity is in turn a function of the turbulence kinetic energy and this energy in its specific form is plotted against the blade length S along the suction and pressure sides in Figs. (3.6 & 3.7). The turbulence kinetic energy is relatively low near the leading edge but higher than the values downstream due to the stagnation conditions at LE and freestream turbulence present in the flow downstream of the LE. As we go downstream, the turbulence kinetic energy decreases and remains very low for the suction side indicating the development of a laminar boundary layer. For the pressure side, the boundary layer develops as laminar and starts to slowly transition at about S = 30 [mm] which can be seen in Fig. 3.7. The turbulence kinetic energy shows an increase from about S = 30mm on the pressure side which confirms the same.

Towards the trailing edge, a common trend is observed for both the suction and pressure sides. Before discussing about the turbulence and heat transfer, attention should be directed to Fig. 3.3. which shows a velocity vector plot of this test case at the trailing edge. The region near the trailing edge sees two separate streams mixing with each other and a wake region is formed. This in fact propagates ahead to form a series of paired vortices similar to a Karman Street Vortex Shedding in the wake region of air-flow behind a cylinder. Since the Turbulence Model employed is a form of RANS model, the complete vortex street could not be visualized in the freestream. A complete LES model will obtain a better prediction for this (Collado, 2018). Nevertheless, a CRVP can be seen near the trailing edge in Fig. 3.3.

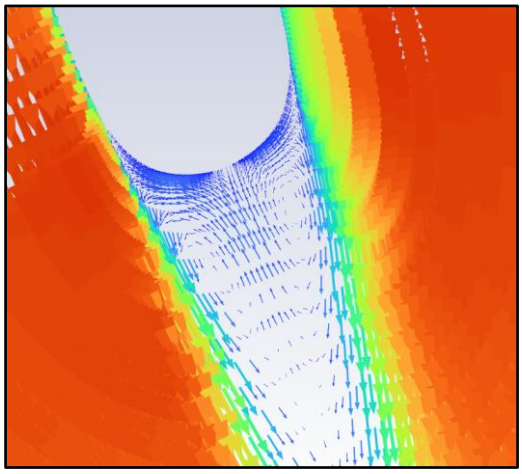

Fig 3.3. Velocity vector plot at the trailing edge

Thus, the trailing edge experiences higher convection and hence, more heat transfer, which explains the sharp upward trend of the heat transfer coefficient towards the trailing edge for both the suction and pressure sides (S = 70 mm for suction side and S = 58 mm for the pressure side).

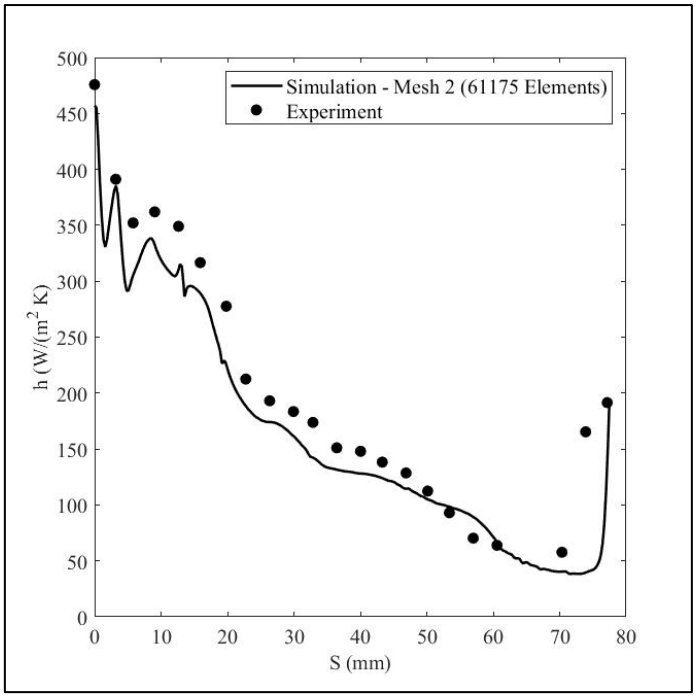

Fig 3.4. Htc distribution along the suction side of the blade for test case 1

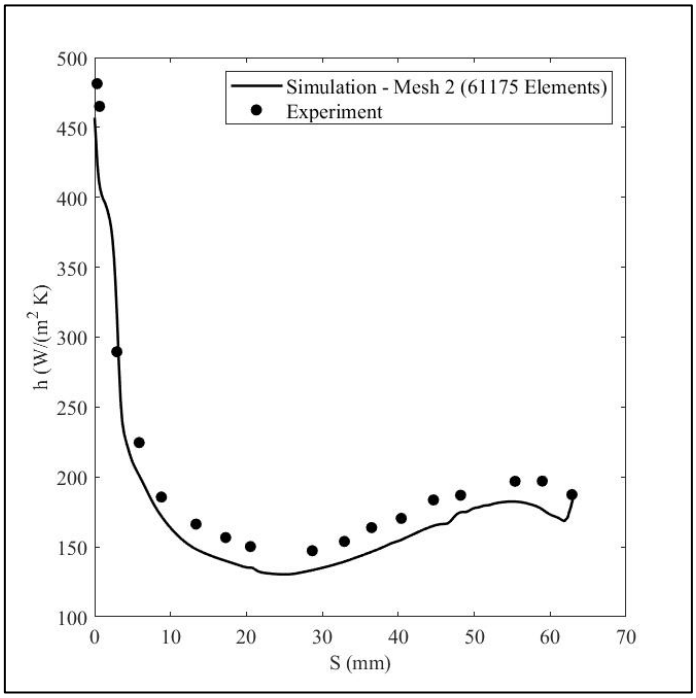

Fig 3.5. Htc distribution along the pressure side of the blade for test case 1

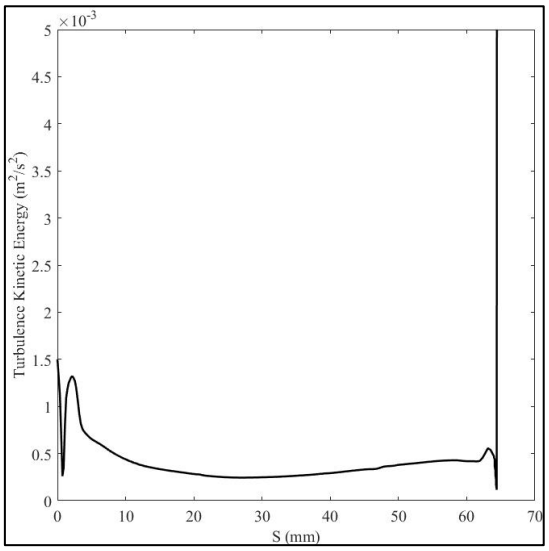

Fig 3.6. Pressure side TKE test case 1

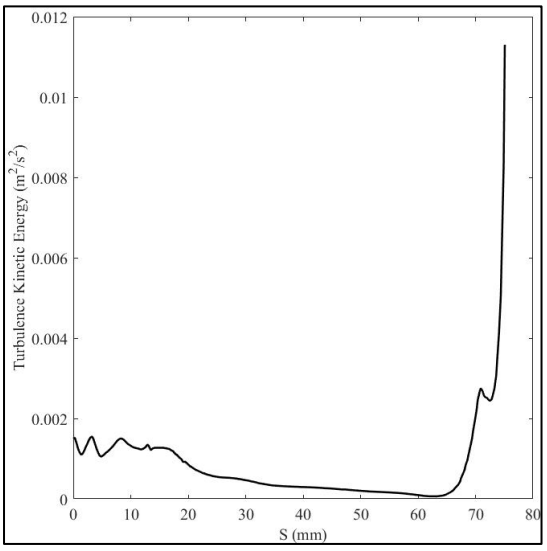

Fig 3.7. Suction side TKE test case 1

The Mach number contour in Fig. 3.8. shows how the flow accelerates fast through the nozzle guide vane and the wake can be seen clearly. This Fig shows the cascade blade with an applied translational periodicity to give the reader a better overview of the flow through the vane between the pressure side of the blade on top and the suction side of the blade below.

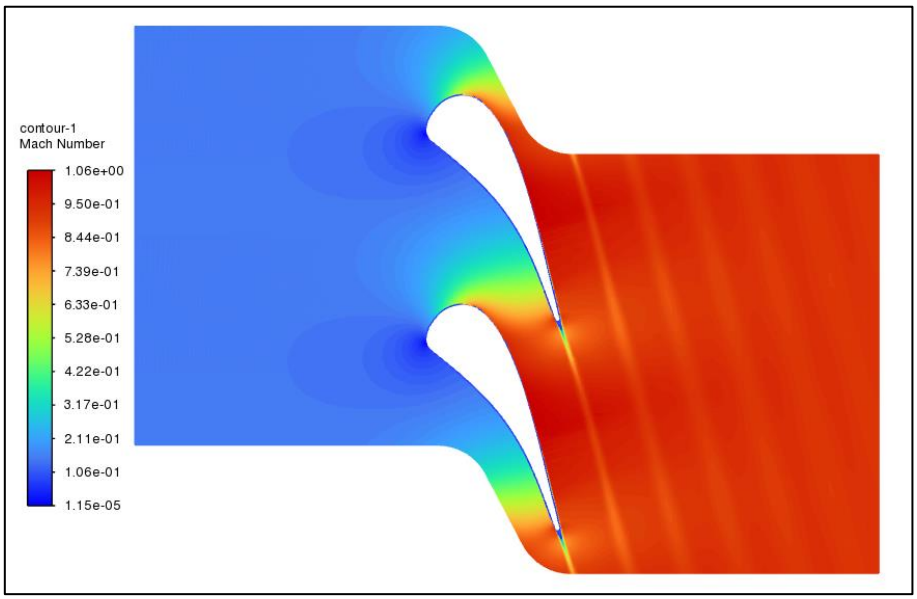

Fig 3.8. Mach number contour plot for the test case 1

Test case 2

The boundary conditions for the test case 2 are presented in the table 3.2 below.

Table. 3.2. BC for the test case 2

Inlet	Total Pressure: 147700 Pa Total Temperature: 420 K Freestream Intermittency: 1 Turbulent Intensity: 3% Turbulent Viscosity Ratio: 10
Outlet	Static Pressure: 88500 Pa
Walls	No Slip BC Temperature: Adiabatic Wall
Periodicity	Conformal Translational Periodicity
Reference Pressure	0 Pa

Comparisons of the obtained numerical prediction with the experimental data are shown in the Figs 3.9. and 3.10. for the suction and pressure sides respectively. On the suction side, the flow accelerates and sees a steep climb up to a Mach number equal to 1.03. After this, the flow decelerates to a Mach number of about 0.85 and suddenly rises up and fluctuates. This region is the wake region near the trailing edge.

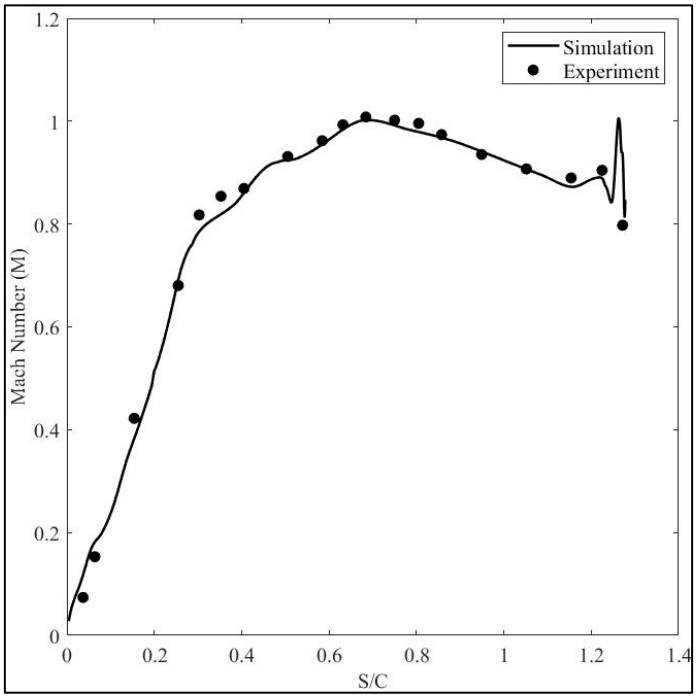

Fig 3.9. Comparison of the numerically obtained blade velocity distributions with the experimental data on the suction side for test case 2

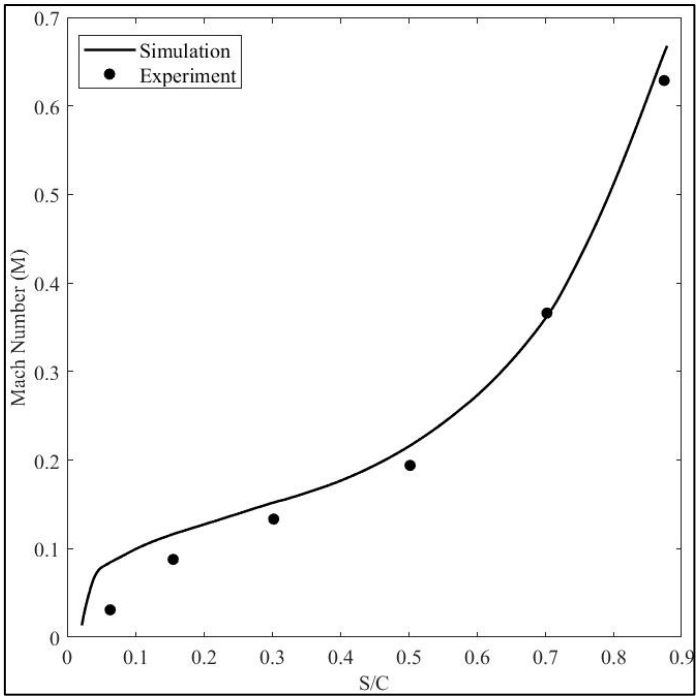

Fig 3.10. Comparison of the numerically obtained blade velocity distributions with the experimental data on the pressure side for test case 2

The TKE along the wall has been shown in Figs. (3.11 & 3.12) for the suction and pressure side respectively. As usual, the trailing edge region sees a higher turbulence intensity and kinetic energy due to the wake region created by the mixing of two streams. Relative to the test case 1, the overall turbulence kinetic energy near the wall is slightly higher but this is owed to the higher Reynold's number of this test case. Unlike the test case 1, the pressure side boundary layer starts to transition into a turbulent boundary layer at about S = 25 mm. The climb of the turbulence level is higher too relative to the test case 1. The suction side boundary layer remains laminar up to the trailing edge region and the trend is very similar to the test case 1.

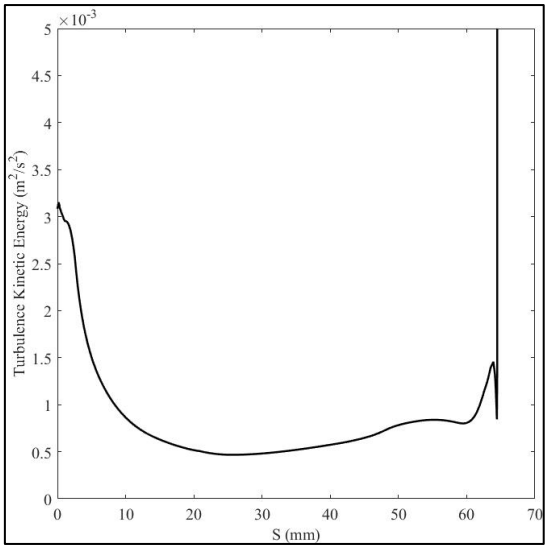

Fig 3.11. Pressure Side TKE for Test 2

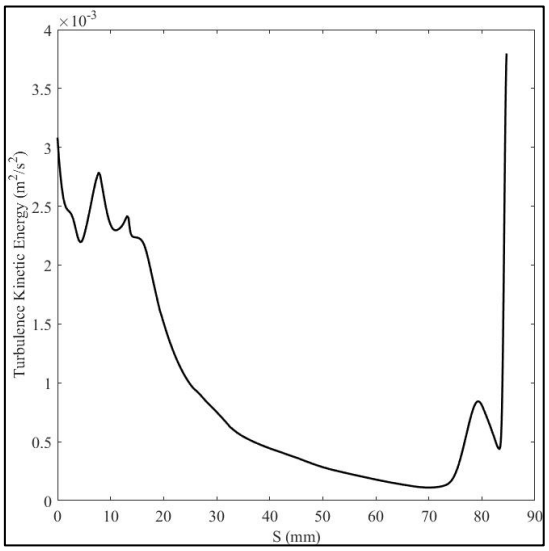

Fig 3.12. Suction Side TKE for Test 2

The Mach number distribution is rather smooth for both the suction and pressure sides as there is no adverse pressure gradient (shock) in the converging section formed by the suction and pressure sides of two blades. An image of the Mach number plot can be found in Fig. 3.13 which shows the presence of the trailing edge vortex shedding but no presence of (even weak) Mach waves/shocks.

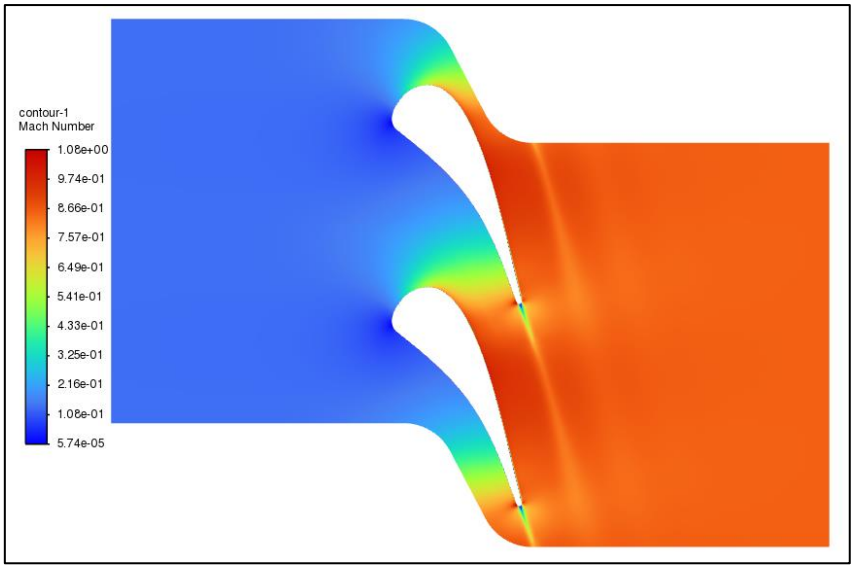

Fig 3.13. Mach number contour plot for the test case 2

Test case 3

The boundary conditions for the test case 3 are presented in the table 3.3 below.

Table. 3.3. BC for the test case 3

Inlet	Total Pressure: 160800 Pa Total Temperature: 420 K Freestream Intermittency: 1 Turbulent Intensity: 3% Turbulent Viscosity Ratio: 10
Outlet	Static Pressure: 82000 Pa
Walls	No Slip BC Temperature: Adiabatic Wall
Periodicity	Conformal Translational Periodicity
Reference Pressure	0 Pa

The numerical predictions plotted against the experimental data are shown in the Figs. (3.14 & 3.15) for the suction and pressure sides respectively. This is an interesting test case as there is a shock which is formed inside the flow. However, the shock does not seem to have any adverse effect on the boundary layer due to its location of occurrence being well downstream of the leading edge and rather towards to trailing edge. In fact, the boundary layer seems to be laminar

over almost the entire length of the suction side. The boundary layer starts to transition, in contrast to the test cases 1 and 2, much earlier on along the pressure side, i.e., about S = 22mm. The leading edge does not experience much fluctuations in the turbulence levels as seen in the test case 2. Air accelerates and speeds up to a Mach number of 1.23 along the suction and post the shock at S/C = 1.1, the flow experiences a sudden pressure gradient and slows down. Upon careful observation, one might notice that the difference in the velocities towards the trailing edge for the streams of air coming from the suction and pressure sides is lesser ($\Delta M_{is} = 0.12$) in contrast to the test case 2 where this difference is relatively more ($\Delta M_{is} = 0.18$). This causes the wake to be weak and it dissipates off faster. Further, the shock-wave from the suction side of the blade interacts with this wake as it finally vanishes off. This can be visualized in Figs. (3.16 & 3.17).

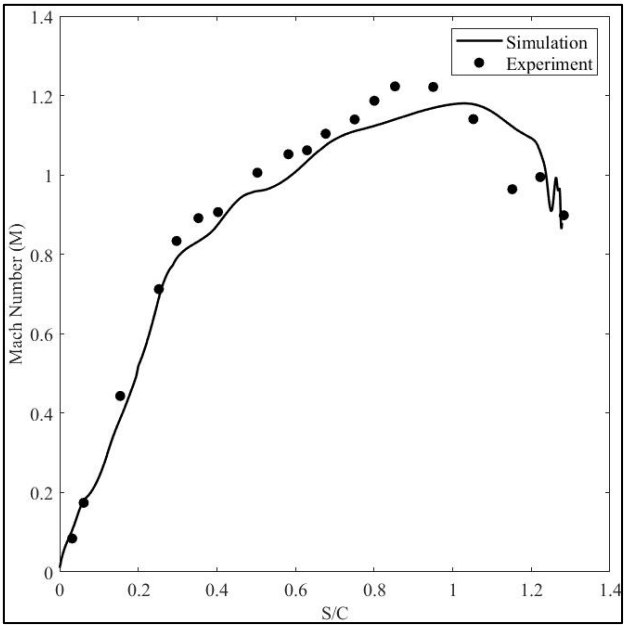

Fig 3.14. Comparison of the numerically obtained blade velocity distributions with the experimental data on the suction side for test case 3

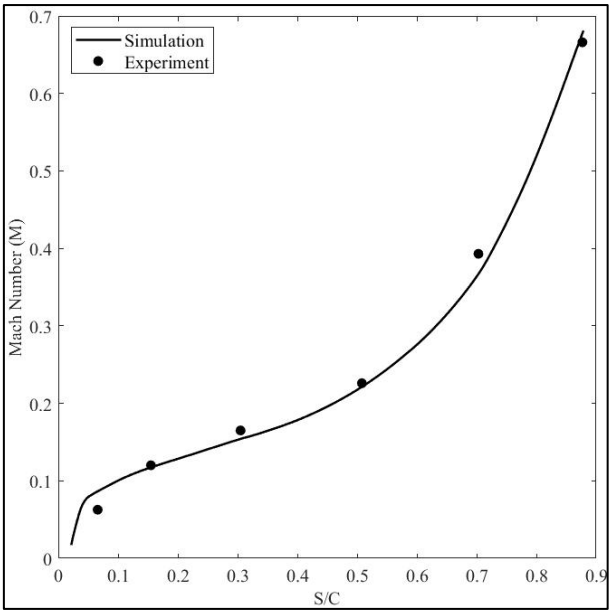

Fig 3.15. Comparison of the numerically obtained blade velocity distributions

with the experimental data on the pressure side for test case 3

For the test 3, Arts et al. (Arts et al., 1990) presented a schlieren flow experimentally obtained visual shown in Fig. 3.16 (a). Fig. 3.16 (b) portrays a Schlieren Flow Visualization (Density gradient-based shadowgraph) for the same test case 3, obtained numerically. The density gradient based shadowgraph was obtained using the equn 14.

$$Gradient(\rho) = \sqrt{\left(\frac{\partial \rho}{\partial x}\right)^2 + \left(\frac{\partial \rho}{\partial y}\right)^2} \quad \ldots (14)$$

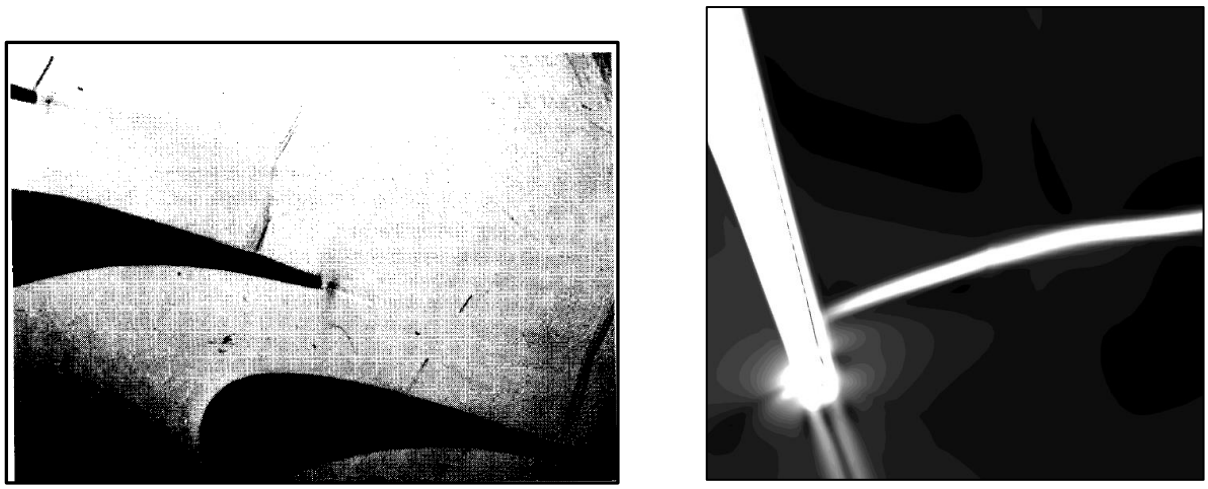

(a) (b)

Fig 3.16. A comparison between the Schlieren flow visual from Arts et al (Arts et al., 1990) (a) and the density gradient based shadowgraph obtained numerically (b)

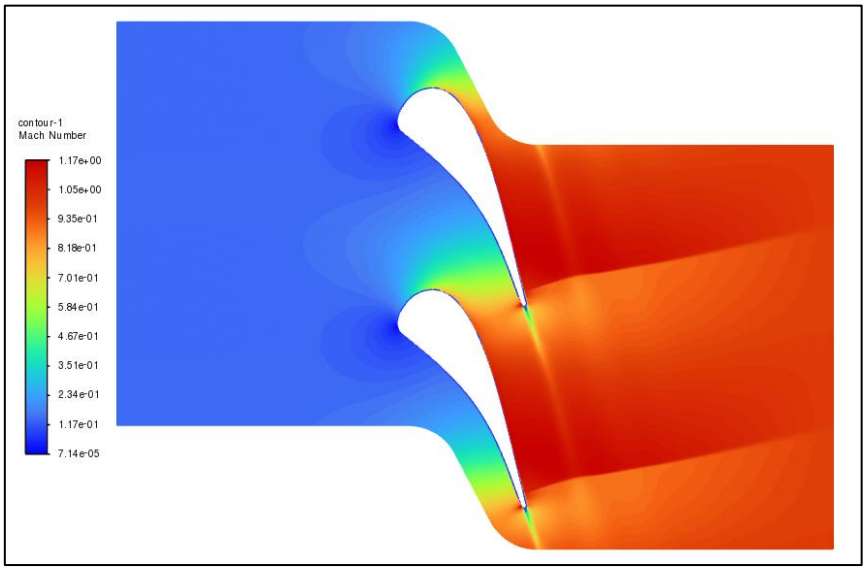

Fig 3.17. Mach number contour plot for the test case 3

3.2 Cooled cases

In this section, the numerical data obtained from simulations is compared with the experimental film cooling data. The experiment case numbers and their corresponding characterizing variables have been listed in Table. 3. With reference to this, the following sub sections have been laid down.

Suction side cooled test case 4

The boundary conditions for the test case 4 are given below in table 3.4.

Table. 3.4. BC for the test case 4

Inlet	Total Pressure: 2.5 bar Total Temperature: 420 K Freestream Intermittency: 1 Turbulent Intensity: 80% Turbulent Viscosity Ratio: 100
Outlet	Static Pressure: 1.6 bar
Walls Suction side and Pressure side	No Slip BC Temperature: Isothermal BC, 300K
Walls of the tubes	No slip, Adiabatic
Inlet to tubes	Velocity inlet BC 130 m/s

The mesh independent solution was plotted against the experimental data. This can be seen in Fig. 3.18.

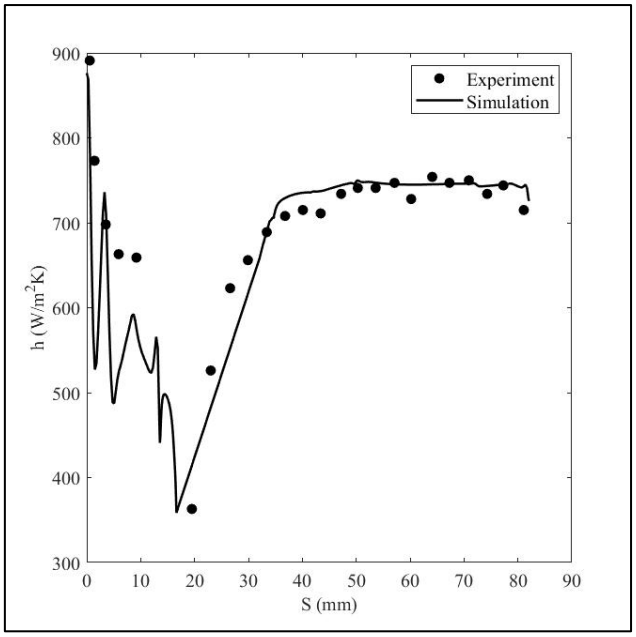

Fig 3.18. Comparison between the experimental and numerically obtained film cooling htc distributions along the suction side for the test case 4.

The prediction was made using the Transition SST model for the suction side cooling, which predicted the transitional state of the boundary layer well. The htc sees a steep decrease in its value from the leading till the location of the hole (S = 14 [mm]), after which there is a region of separation which can be seen in the velocity streamlines contour in Fig. 3.19 (a), plotted at the mid-plane. The fluid jets out of the cooling hole and a region of separation can be seen right next to the hole. Further, the horizontal velocity component contour plot in Fig. 3.19 (b) shows that its value is very high in the region near the hole, indicating a separation and increasing turbulence intensity, which is further confirmed by the TKE plot in Fig. 3.20. The flow then re-attaches to the surface at about (S = 32[mm]) and remains in a transitional state till the trailing edge.

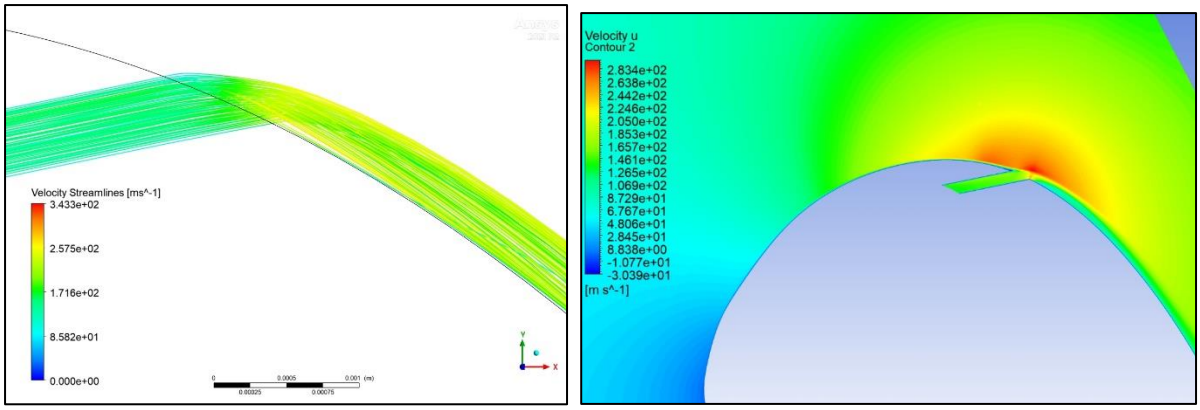

(a) (b)

Fig 3.19. Velocity streamlines exiting the circular hole (a) and the horizontal velocity component plot (b)

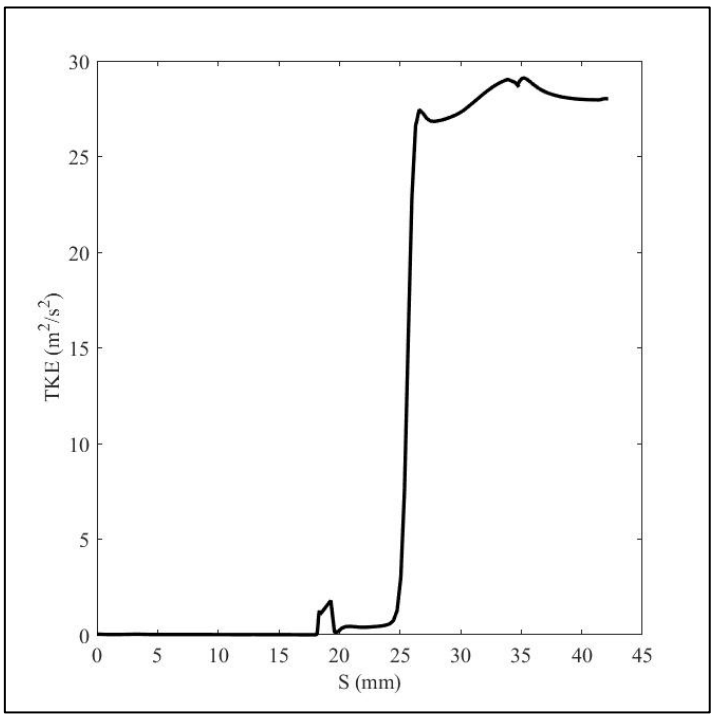

Fig 3.20. TKE plot for the suction side cooled test case 4

The TKE plot from Fig. 3.20 shows that the htc is initially high due to stagnation of air near the leading edge and downstream of the holes, the turbulence intensity increases due to the jetting action of the coolant which essentially impinges into the boundary layer. The flow further downstream of the holes then tends to laminarize but remains in a transitional state.

Pressure side cooled test case 5

The boundary conditions for the test case 5 are given below in table 3.5.

Table. 3.5. BC for the test case 5

Inlet	Total Pressure: 2.5 bar Total Temperature: 420 K Freestream Intermittency: 1 Turbulent Intensity: 80% Turbulent Viscosity Ratio: 100
Outlet	Static Pressure: 1.6 bar
Walls Suction side and Pressure side	No Slip BC Temperature: Isothermal BC, 300K
Walls of the tubes	No slip, Adiabatic
Inlet to tubes	Velocity inlet BC. 50 m/s

The mesh independent solution is plotted against the experimental data in Fig. 3.21. This prediction was made using the k-w SST model. The transition SST model failed to predict the HTC distribution, as can be seen in Fig. 3.21. The turbulence onset just after the cooling hole tends to transition into a turbulent boundary layer. Downstream of the cooling holes, the boundary layer can be seen to be transitioning into fully turbulent as is evident from Fig. 3.21, wherein the heat transfer coefficient sees a steady rise in its value along the blade length. The TKE plot (Fig. 3.22) re-affirms this phenomenon.

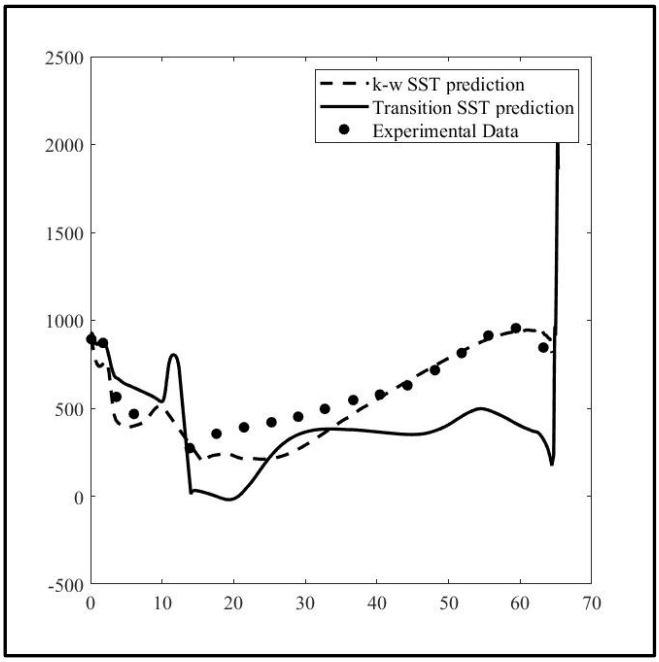

Fig 3.21. Comparison between the htc values from

Transition SST, k-w SST and the experiment for test case 5

The Transition SST model tends to laminarize the boundary layer just after the cooling holes. Tuning the model input parameters such as F_{onset} and the momentum thickness-based Reynold's numbers could help in a better prediction. In Fluent, the model coefficients are evaluated numerically using proprietary empirical relations using the F_{onset}, momentum thickness-based Reynold's number Re_{theta} and F_{length}. The parameters can be input manually as well. Nevertheless, the Menter's k-w SST model predicts this fairly well.

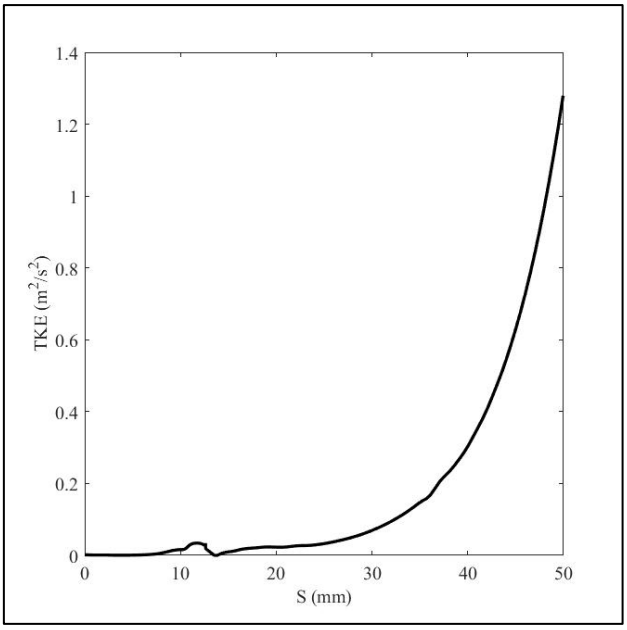

Fig 3.22. TKE plot for test case 5

The TKE plot is shown in Fig. 3.22 for the test case 5. The increase in turbulence intensity is rather smoother for the pressure side in contrast to the suction side when the blade is being cooled. However, the aggregate TKE remains relatively low as compared to the suction side case. This is because the fluid is relatively slower over the pressure side due to opposite velocity gradients from the wall into the freestream for the suction and pressure sides. The air then achieves static temperature values leaning towards the total temperature of the flow. This increased difference in temperatures between the wall and the freestream causes the heat transfer to go higher. Hence, the htc values for each side are comparable, whilst the TKE values are not.

3.3 Comparison between the performance of 777 and circular holes

The coolant conditions such as the injection angle, blowing ratios, etc., were kept the same in the case of the 777-hole when comparing with the circular holes. Hence, the BCs were also the exact same. The htc comparison plot between the two holes can be seen in Fig. 3.23 (a & b), for the pressure and suction sides respectively. The TKE plots can be seen in Fig. 3.24 (a & b) for the pressure and suction sides respectively. The cooling performance of the 777-hole is good for the pressure side, whilst on the suction side, the performance drops and leads to higher htc values than the circular hole after S = 39 [mm].

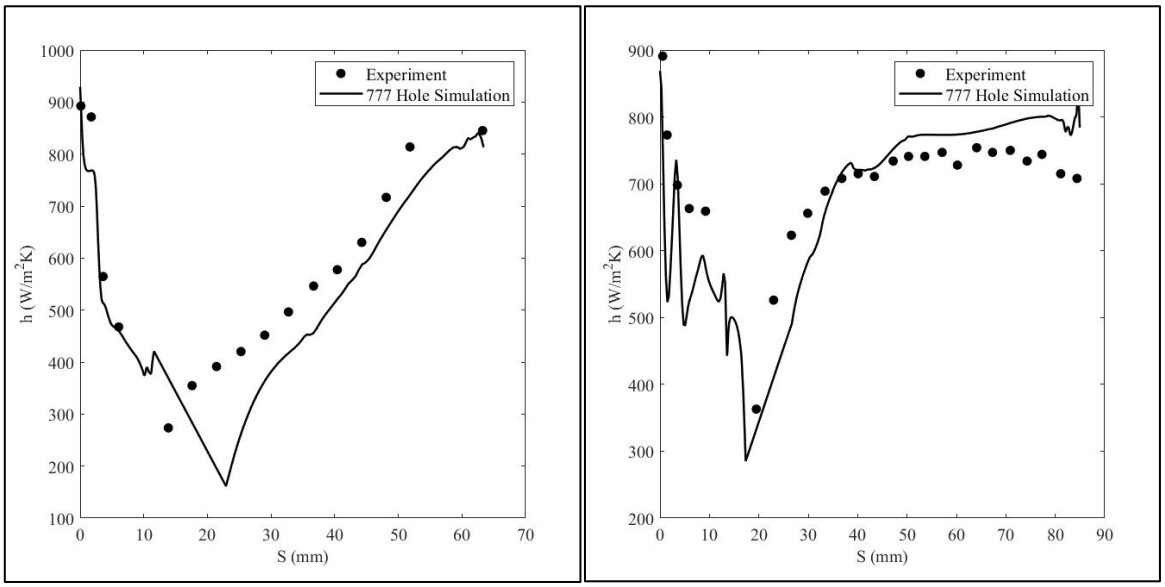

(a) (b)

Fig 3.23. Comparison of the 777-hole htc distributions for the pressure side (a) and the suction side (b)

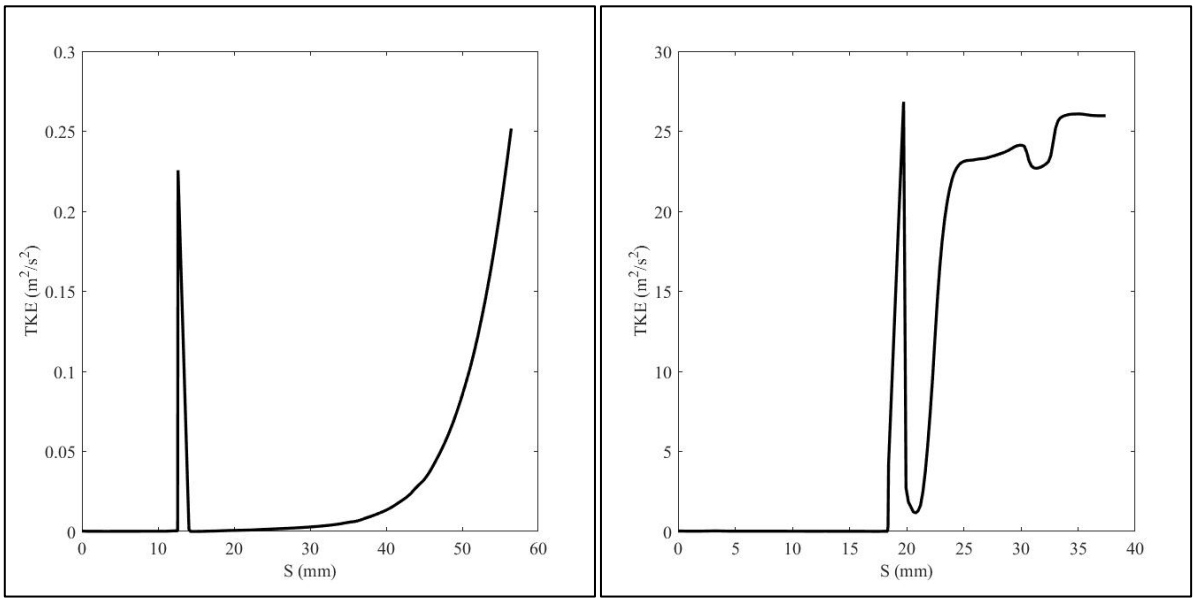

(a) (b)

Fig 3.24. The TKE plots for the 777 cooled pressure side (a) and suction side (b)

For the pressure side cooled by the 777-hole, the htc remains lower than the htc for the circular hole cooled case. Comparing Fig. 3.24 (a) with Fig. 3.21, it can be seen that the TKE increase is delayed in the 777-hole case and hence the boundary layer is in a transitional state for a good length downstream of the 777-hole. The heat flux along the z-direction for the translational periodic length in the span-wise direction has been plotted for the pressure side cooled cases for both the holes (Fig. 3.25). This has been plotted at three different locations downstream of the cooling hole.

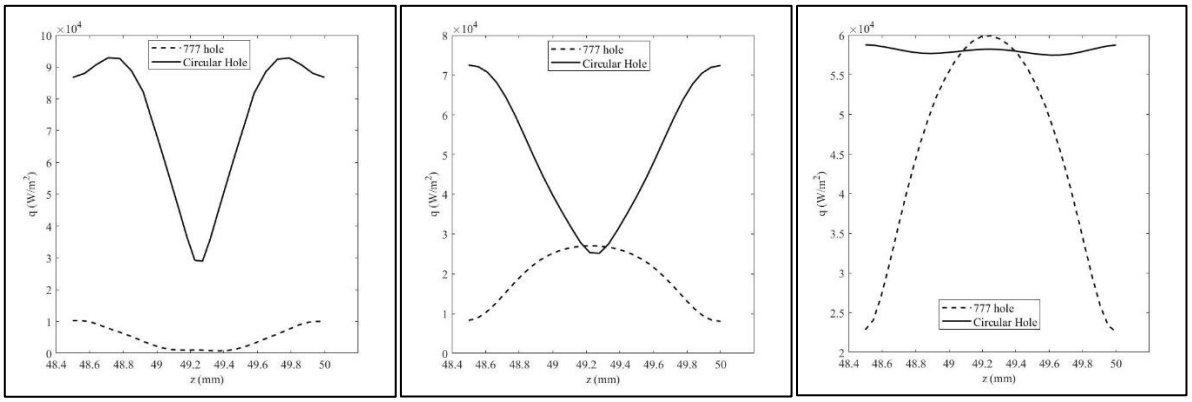

(a) (b) (c)

Fig 3.25. The heat flux vs z direction plots for the pressure side at locations Ca_x = 0.01345m (a); Ca_x = 0.017m (b); Ca_x = 0.025m (c)

Clearly, the 777-hole on an aggregate basis provides better cooling performance on the pressure side. For the suction side, the TKE plot comparison between Fig. 3.24 (b) & Fig. 3.19 reveals that the TKE value increases just after the cooling hole and drops immediately. It then continues to increase and remains in a transitional state. This is because the 777-hole provides very good design for avoiding the flow separation tendencies. The flow can clearly be seen to be slightly detaching and then immediately reattaching to the wall in Fig. 3.27 which showcases the velocity streamlines. This can be compared with the streamlines plot in Fig. 3.18 (a) for the circular hole case, which shows jetting of the coolant and separation tendencies.

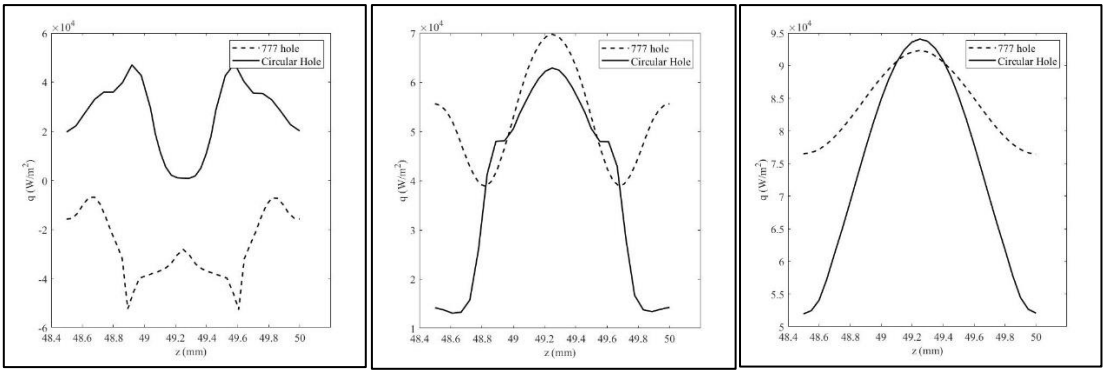

(a) (b) (c)

Fig 3.26. The heat flux vs z direction plots for the suction side at locations

Ca_x = 0.0143m (a); Ca_x = 0.02m (b); Ca_x = 0.025m (c)

The same heat flux plots as Fig. 3.25 have been plotted in Fig 3.26. (a,b &c) for the suction sides, comparing the 777 hole and the circular hole. Initially, the holes provide a good cooling performance. However, downstream of the holes, the turbulence increases and with it, the convective heat transfer. The boundary layer enters into a transitional state again, but at a higher level of heat flux.

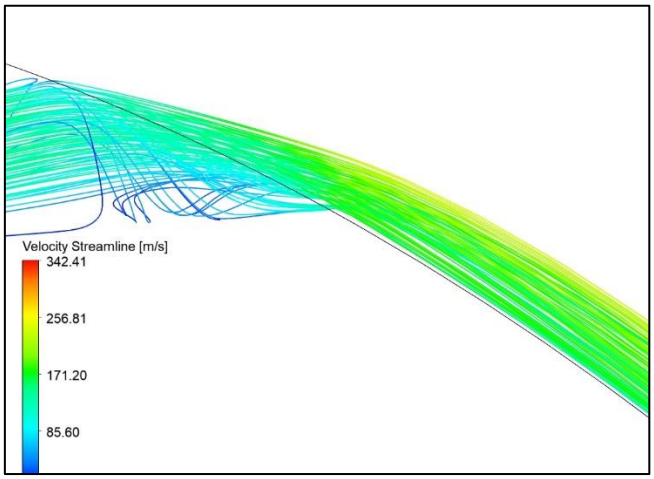

Fig 3.27. Velocity streamline plot for the 777-cooled suction side

In film cooling, the spread of the coolant is of prime importance. A better coolant spread would imply lesser number of holes being drilled into the turbine blade. If the cooling holes provide a good cooling performance for a lesser number of holes, it aids in the structural integrity of the turbine blade, which becomes questionable when a large number of staggered holes are employed. To assess the spread of the coolant in the given case, density contour plots (Figs. 3.28 & 3.29) were made which shows the thickness of the coolant layer entering the freestream for the pressure side and suction side cooled cases for the circular hole shape and the 777-hole

shapes. Next, the heat flux contours for all four cases were plotted on the walls to see the distribution of heat flux into the blade wall at different locations by applying periodicity in the span-wise direction as shown in Fig. 3.30. The readers should note that it would have been convenient to plot the temperature contours instead. However, the validation of the numerical data with the experimental data, as aforementioned in Chapter 2, required that the wall be given an isothermal BC. Hence, the heat flux contours were plotted instead. The heat flux contours show that for the 777-hole shape, the cooling is better on the pressure side and for the suction side, the cooling is initially better and becomes inefficient farther downstream of the 777 cooling holes.

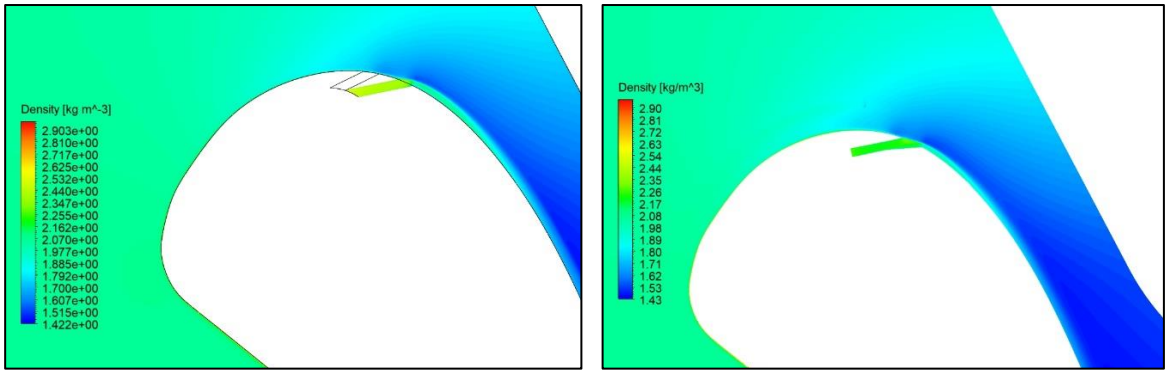

(a) (b)

Fig 3.28. Density contour plots for the suction side cooled by circular hole (a) and the 777-hole (b)

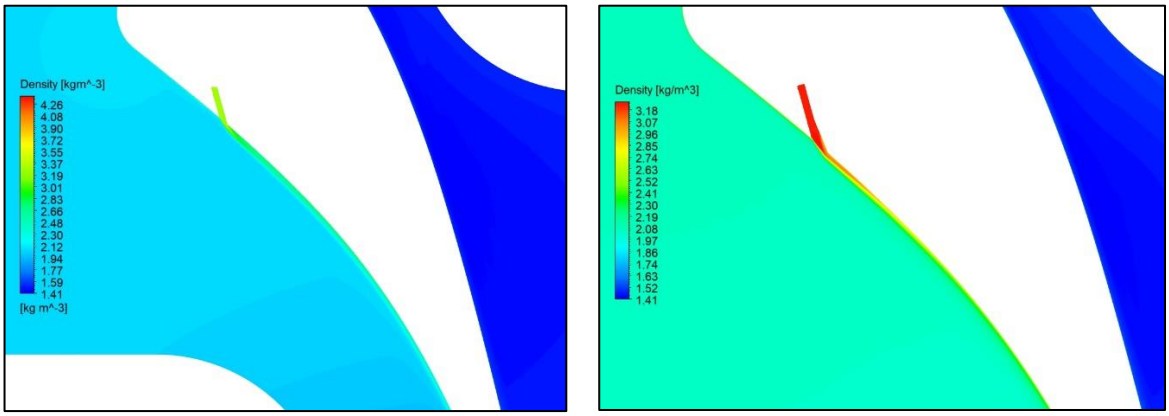

(a) (b)

Fig 3.29. Density contour plots for the pressure side cooled by circular hole (a) and the 777-hole (b)

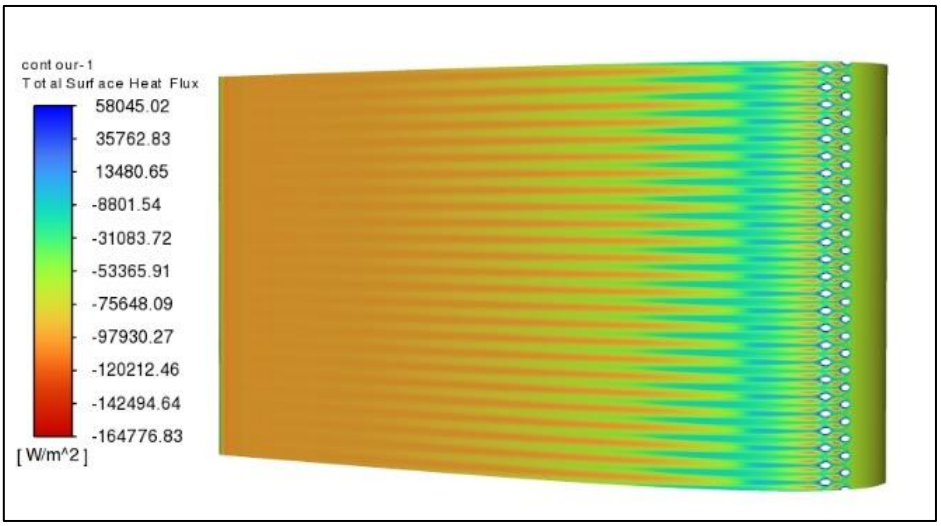
contour-1
Total Surface Heat Flux
58045.02
35762.83
13480.65
-8801.54
-31083.72
-53365.91
-75648.09
-97930.27
-120212.46
-142494.64
-164776.83
[W/m^2]

(a)

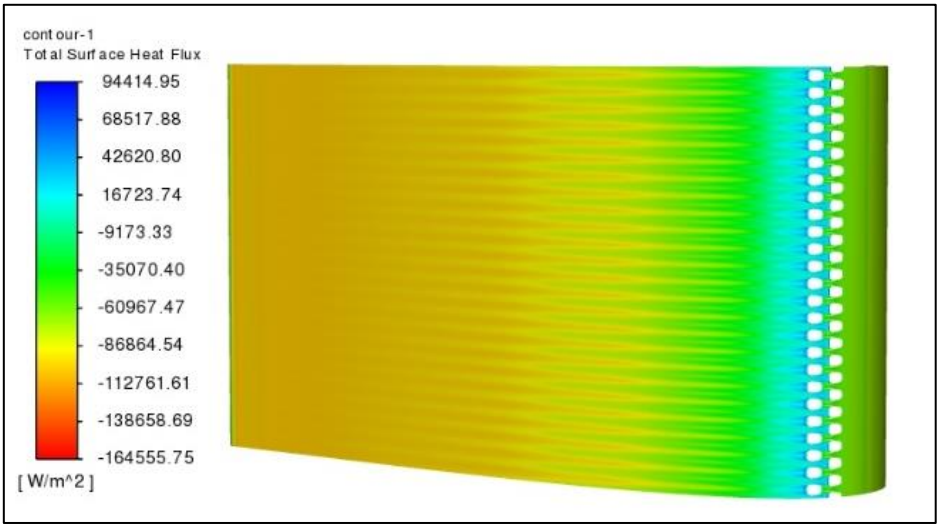
contour-1
Total Surface Heat Flux
94414.95
68517.88
42620.80
16723.74
-9173.33
-35070.40
-60967.47
-86864.54
-112761.61
-138658.69
-164555.75
[W/m^2]

(b)

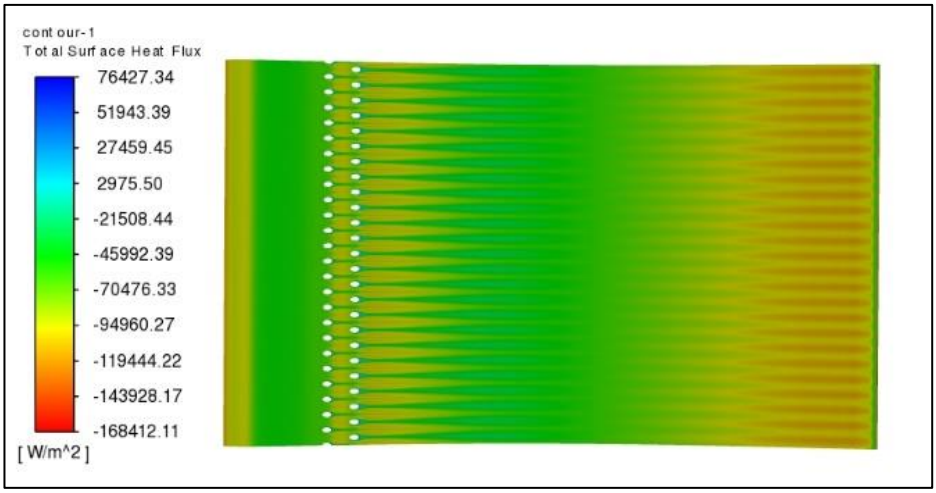
contour-1
Total Surface Heat Flux
76427.34
51943.39
27459.45
2975.50
-21508.44
-45992.39
-70476.33
-94960.27
-119444.22
-143928.17
-168412.11
[W/m^2]

(c)

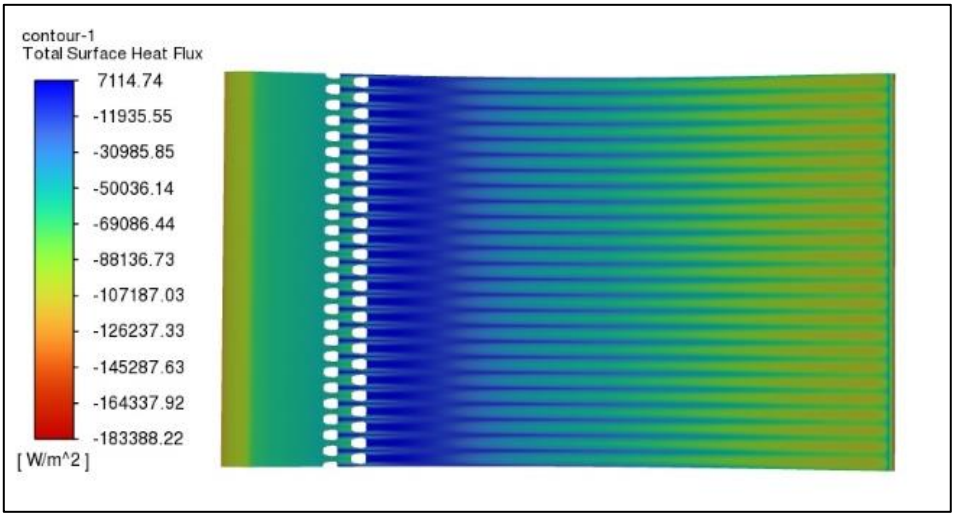

(d)

Fig 3.30. Heat flux contours for the suction side cooled by circular hole (a) and 777-hole (b) and the pressure side cooled by the circular hole (c) and 777-hole (d)

As can be seen from Figs. (3.28 & 3.29), the thickness of the coolant in the circular hole cases is relatively more in contrast to the 777-hole. Three-dimensional streamline plots for both hole types have also been plotted in Fig. 3.31. It is inferred from these Figs that the coolant spread for the 777 hole is much better than that for the circular hole.

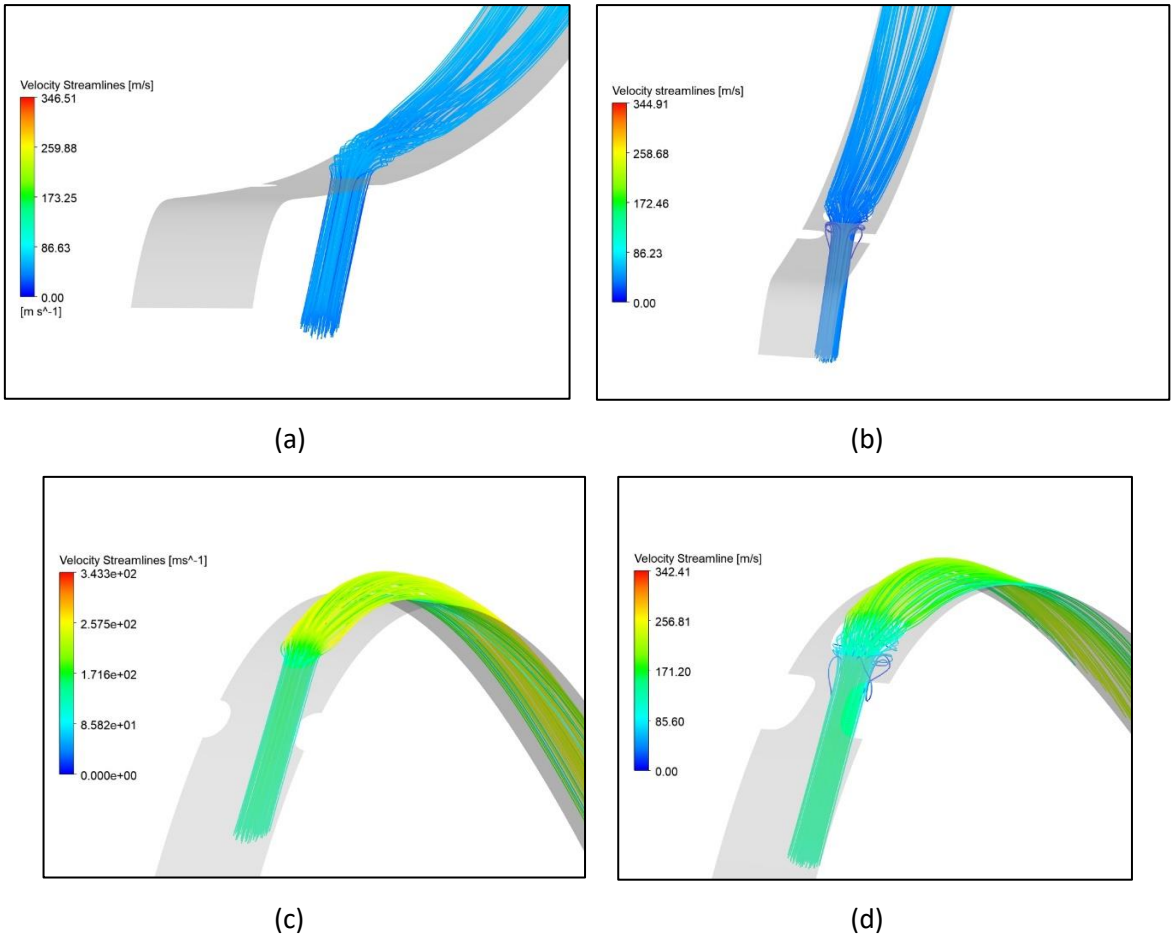

Fig 3.31. Velocity streamlines for the pressure side cooled by circular hole (a) and 777-hole (b) and the suction side cooled by the circular hole (c) and 777-hole (d).

The structural integrity of the 777-cooling case shown is definitely poor as compared to the circular shaped holes because of the number of holes and their size. It was necessary to maintain the similar coolant flow inlet and cooling configuration to compare the holes for the given transonic vane. However, given the coolant spreading and cooling performance as seen from the results, it is evident that for a particular hole size, coolant flow characterizing conditions such as hole location and injection angles, and reduced number of holes, the 777-hole has a very good potential for providing efficient cooling performance for transonic turbine NGVs.

CHAPTER 4
CONCLUSIONS

The flow through the LS89/94 NGV for both the cooled (LS94) and non-cooled (LS89) cases was investigated using ANSYS Fluent. The experimental test cases were chosen and the numerical results were compared with the available experimental datasets for the cooled and non-cooled cases to validate the adopted methodology. Excellent matches were obtained with the experimental datasets for all chosen cases. The validated methodology was then followed to study the effect of changing the hole shape from circular hole to the 777-hole shape. It was inferred from this study that the 777-hole shape has potential in providing enhanced film cooling performance for transonic turbine blades of the type of LS89/94.

In addition to the main conclusions, the relevant outcomes of this study have been given below:

1. The adopted methodology predicted the experimental data well and this methodology of improved prediction potential can be followed to obtain rather realistic predictions.
2. For the non-cooled cases, the Transition SST model worked well. The Transition SST model has a very good prediction potential for transitioning flows of the given type considered in this study.
3. For the cooled cases, the Transition SST model worked well for the suction side but under predicted the heat transfer on the pressure side due to laminarization source terms eating up the turbulence downstream of the cooling hole. The model constants such as Re_{theta}, F_{onset} and F_{length} should be changed in order to obtain a better prediction. However, the k-w SST model predicted the htc distribution well for the cooled pressure side case.
4. Larger inlet turbulence intensity and turbulent viscosity ratio were to be given in order to attain the required turbulence intensity at the LE of the blade due to turbulence decay in the free stream predicted by the SST models.
5. The Mach number does not seem to affect the heat transfer into the vane much as compared to the flow Re number for the given transonic vane.
6. The 777-hole shape has potential in providing efficient cooling in transonic turbine vanes of the type LS89/94. Its cooling effectiveness, coolant spreading and jet

separation avoidance are desirable characteristics, which were observed in the numerical studies.

7. There is scope in further investigations and parametric studies involving the change of different coolant flow characterizing parameters such as injection angle, hole size, hole location and the internal geometric parameters are given in Fig. 2.11, using the current methodology of increased prediction potential and accuracy.

REFERENCES

Arts, T. and Rouvroit, M. L. De, Aero-Thermal Performance of a Two Dimensional Highly Loaded Transonic Turbine Nozzle Guide Vane : A Test Case for Inviscid and Viscous Flow Computations, *Proceedings of the ASME Turbo Expo*, vol. **1**, 1990. DOI: 10.1115/90-GT-358

Asiegbu, L. and Johnsson, R., CFD Based External Heat Transfer Coefficient Predictions on a Transonic Film-Cooled Gas Turbine Guide Vane, 2022.

Bassi, F., Fontaneto, F., Franchina, N., Ghidoni, A. and Savini, M., Turbine Vane Film Cooling: Heat Transfer Evaluation Using High-Order Discontinuous Galerkin RANS Computations, *International Journal of Heat and Fluid Flow*, vol. **61**, pp. 610–25, from http://dx.doi.org/10.1016/j.ijheatfluidflow.2016.07.007, 2016. DOI: 10.1016/j.ijheatfluidflow.2016.07.007

Bogard, D. G., Airfoil Film Cooling, *The Gas Turbine Handbook*, pp. 309–21, from http://www.netl.doe.gov/technologies/coalpower/turbines/refshelf/handbook/4.2.2.1.pdf, 2006.

Dees, J. E., Bogard, D. G., Ledezma, G. A., Laskowski, G. M. and Tolpadi, A. K., Momentum and Thermal Boundary Layer Development on an Internally Cooled Turbine Vane, *Journal of Turbomachinery*, vol. **134**, no. 6, pp. 1–11, 2012. DOI: 10.1115/1.4006281

Dyson, T. E., Bogard, D. G., Piggush, J. D. and Kohli, A., Overall Effectiveness for a Film Cooled Turbine Blade Leading Edge with Varying Hole Pitch, *Journal of Turbomachinery*, vol. **135**, no. 3, pp. 1–8, 2013. DOI: 10.1115/1.4006872

Phan, H. M., Duan, P. H. and Dinh, C. T., Numerical Aero-Thermal Study of High-Pressure Turbine Nozzle Guide Vane: Effects of Inflow Conditions, *Physics of Fluids*, vol. **32**, no. 3, from https://doi.org/10.1063/1.5144418, 2020. DOI: 10.1063/1.5144418

Schroeder, R. P. and Thole, K. A., Adiabatic Effectiveness Measurements for a Baseline Shaped Film Cooling Hole, *Proceedings of the ASME Turbo Expo*, vol. **5B**, pp. 1–13, 2014. DOI: 10.1115/GT2014-25992

Studi, D., Bergamo, D. I., Industriale, I. and Ricerca, D. D. I., Aero-Thermal Performance of a Film-Cooled High Pressure Turbine Blade / Vane: A Test Case for Numerical Codes Validation, pp. 1–202, 2014.

Torreguitart, I. S., Verstraete, T. and Mueller, L., Optimization of the LS89 Axial Turbine Profile Using a Cad and Adjoint Based Approach, *International Journal of Turbomachinery, Propulsion and Power*, vol. **3**, no. 3, pp. 1–13, 2018. DOI: 10.3390/ijtpp3030020

Yavari, H., Khavari, A., Alizadeh, M., Kashfi, B. and Khaledi, H., Aero-Thermal Redesign of a High Pressure Turbine Nozzle Guide Vane, *Propulsion and Power Research*, vol. **8**, no. 4, pp. 310–19, 2019. DOI: 10.1016/j.jppr.2019.01.012

rohit_verified

ORIGINALITY REPORT

12%	8%	11%	1%
SIMILARITY INDEX	INTERNET SOURCES	PUBLICATIONS	STUDENT PAPERS

PRIMARY SOURCES

1	F. Bassi, F. Fontaneto, N. Franchina, A. Ghidoni, M. Savini. "Turbine vane film cooling: Heat transfer evaluation using high-order discontinuous Galerkin RANS computations", International Journal of Heat and Fluid Flow, 2016 Publication	1%
2	repository.tudelft.nl Internet Source	1%
3	hdl.handle.net Internet Source	1%
4	oatao.univ-toulouse.fr Internet Source	1%
5	Unsteady Aerodynamics and Aeroelasticity of Turbomachines, 1998. Publication	<1%
6	liu.diva-portal.org Internet Source	<1%
7	www.diva-portal.se Internet Source	<1%

8	www.tandfonline.com Internet Source	<1 %
9	Submitted to City University Student Paper	<1 %
10	aip.scitation.org Internet Source	<1 %
11	www.ijert.org Internet Source	<1 %
12	Stefano Gaggero, Diego Villa. "Improving model scale propeller performance prediction using the k − k L − ω transition model in OpenFOAM", International Shipbuilding Progress, 2018 Publication	<1 %
13	William Wolf, Sanjiva Lele, Giridhar Jothiprasad, Lawrence Cheung. "Investigation of Noise Generated by a DU96 Airfoil", 18th AIAA/CEAS Aeroacoustics Conference (33rd AIAA Aeroacoustics Conference), 2012 Publication	<1 %
14	arc.aiaa.org Internet Source	<1 %
15	Para, Srinivasa Rao, Xianchang Li, and Ganesh Subbuswamy. "Numerical Study of Mist Film Cooling in Combustor at Operating Conditions", Volume 9 Heat Transfer Fluid	<1 %

Flows and Thermal Systems Parts A B and C, 2009.
Publication

16	Rutledge, James L., Marc D. Polanka, and David G. Bogard. "The Delta Phi Method of Evaluating Overall Film Cooling Performance", Volume 5B Heat Transfer, 2015. Publication	<1 %
17	Sarkar, S.. "Analysis of transitional flow and heat transfer over turbine blades: Algebraic versus low-Reynolds-number turbulence model", Proceedings of the Institution of Mechanical Engineers Part C Journal of Mechanical Engineering Science, 2001. Publication	<1 %
18	Wright, Lesley M., Sarah A. Blake, Dong-Ho Rhee, and Je-Chin Han. "Effect of Upstream Wake With Vortex on Turbine Blade Platform Film Cooling With Simulated Stator-Rotor Purge Flow", Volume 4 Turbo Expo 2007 Parts A and B, 2007. Publication	<1 %
19	pureadmin.qub.ac.uk Internet Source	<1 %
20	www.politesi.polimi.it Internet Source	<1 %

21	Barigozzi, Giovanna, Giuseppe Franchini, Antonio Perdichizzi, Massimiliano Maritano, and Roberto Abram. "Purge flow and interface gap geometry influence on the aero-thermal performance of a rotor blade cascade", International Journal of Heat and Fluid Flow, 2013. Publication	<1 %
22	Feng Han, Hong Guo, Xiao-feng Ding, Da-wei Zhang, Hai-wang Li. "Experimental investigation on the effects of hole pitch and blowing ratio on the leading edge region film cooling of a rotating twist turbine blade", International Journal of Heat and Mass Transfer, 2020 Publication	<1 %
23	Hannes Fulge, Andreas Knapp, Ricarda Wernitz, Christoph Eichhorn, Georg Herdrich, Stefanos Fasoulas, Stefan Lohle. "Improved Abel Inversion Method for Analysis of Spectral and Photo-Optical Data of Magnetic Influenced Plasma Flows", 42nd AIAA Plasmadynamics and Lasers Conference, 2011 Publication	<1 %
24	Huilan Yao, Huaixin Zhang. "A simple method for estimating transition locations on blade surface of model propellers to be used for calculating viscous force", International	<1 %

Journal of Naval Architecture and Ocean Engineering, 2017
Publication

25	www.edm2.com Internet Source	<1 %
26	A. Arab, M. Javadi, M. Anbarsooz, M. Moghiman. "A numerical study on the aerodynamic performance and the self-starting characteristics of a Darrieus wind turbine considering its moment of inertia", Renewable Energy, 2017 Publication	<1 %
27	S. Pröbsting, J. Serpieri, F. Scarano. "Experimental investigation of aerofoil tonal noise generation", Journal of Fluid Mechanics, 2014 Publication	<1 %
28	Sumanta Acharya, Yousef Kanani. "Advances in Film Cooling Heat Transfer", Elsevier BV, 2017 Publication	<1 %
29	openscholarship.wustl.edu Internet Source	<1 %
30	Pascale Kulisa, Cédric Dano. "Assessment of linear and non-linear two-equation turbulence models for aerothermal turbomachinery flows", Journal of Thermal Science, 2006 Publication	<1 %

31	Wu, Hong, S. Nasir, W. F. Ng, and H. K. Moon. "Showerhead Film Cooling Performance of a Transonic Turbine Vane at High Freestream Turbulence (Tu = 16%): 3-D CFD and Comparison With Experiment", Volume 10 Heat Transfer Fluid Flows and Thermal Systems Parts A B and C, 2008. Publication	<1 %
32	apps.dtic.mil Internet Source	<1 %
33	Dyson, Thomas E., David G. Bogard, and Sean D. Bradshaw. "A CFD Evaluation of Multiple RANS Turbulence Models for Prediction of Boundary Layer Flows on a Turbine Vane", Volume 3C Heat Transfer, 2013. Publication	<1 %
34	Kh Javadi, M Taeibi-Rahni, M Darbandi. "Jet into Cross Flow Boundary Layer Control - An Innovation in Gas Turbine Blade Cooling", 35th AIAA Fluid Dynamics Conference and Exhibit, 2005 Publication	<1 %
35	Pietro Formisano, Tânia S. Cação Ferreira, Tony Arts. "Influence of the Gas-to-Wall Temperature Ratio on the Boundary Layer Transition: Investigation of the Wake Behind a	<1 %

Turbine Nozzle Guide Vane", Volume 2B: Turbomachinery, 2019
Publication

36	W.L. Chen, F.S. Lien, M.A. Leschziner. "Computational prediction of flow around highly loaded compressor-cascade blades with non-linear eddy-viscosity models", International Journal of Heat and Fluid Flow, 1998 Publication	<1 %
37	Wu, Hong, Yusheng Liu, and Guoqiang Xu. "Measurements of heat transfer and pressure in a trailing edge cavity of a turbine blade", Chinese Journal of Aeronautics, 2013. Publication	<1 %
38	www.mdpi.com Internet Source	<1 %
39	www.researchgate.net Internet Source	<1 %
40	Qingkai Zhao, Tao Chen, Wei Xiao, Xiangbin Chen, Xiongliang Yao, Wenpu Wang. "Research on the characteristics of cavitation flow and pressure load during vertical water exit of different head-shaped vehicles", Ocean Engineering, 2022 Publication	<1 %

41	T. W. Simon, J. D. Piggush. "Turbine Endwall Aerodynamics and Heat Transfer", Journal of Propulsion and Power, 2006 Publication	<1 %
42	Submitted to Wright State University Student Paper	<1 %
43	ntnuopen.ntnu.no Internet Source	<1 %
44	A. Boudjir, T. J. Craft, A. Turan. "Computational Investigation of Flow through a Rotating Square Duct by Means of Advanced Second-moment Closure", Flow, Turbulence and Combustion, 2007 Publication	<1 %
45	International Journal of Numerical Methods for Heat & Fluid Flow, Volume 16, Issue 4 (2006-09-19) Publication	<1 %
46	Je-Chin Han, Srinath Ekkad. "Recent Development in Turbine Blade Film Cooling", International Journal of Rotating Machinery, 2001 Publication	<1 %
47	N Suryavamshi. "Three-dimensional flow field downstream of an embedded stator in a multistage axial flow compressor: Part 2: deterministic stress and heat flux distribution	<1 %

and average-passage equation system", Proceedings of the Institution of Mechanical Engineers Part A Journal of Power and Energy, 01/01/2001
Publication

48	Shaofei Zheng, Yidan Song, Gongnan Xie, Bengt Sunden. "AN ASSESSMENT OF TURBULENCE MODELS FOR PREDICTING CONJUGATE HEAT TRANSFER FOR A TUBINE VANE WITH INTERNAL COOLING CHANNELS", Heat Transfer Research, 2015 Publication	<1 %
49	jjmie.hu.edu.jo Internet Source	<1 %
50	www.rotordynamics.org Internet Source	<1 %

Exclude quotes	On	Exclude matches	< 10 words
Exclude bibliography	On		

Sustainable Development Goals related to the Project

SDG No	SDG Description	Yes/No
1	Eliminate Poverty	No
2	Erase Hunger	No
3	Establish Good Health and Well-Being	No
4	Provide Quality Education	No
5	Enforce Gender Equality	No
6	Improve Clean Water and Sanitation	No
7	Grow Affordable and Clean Energy	No
8	Create Decent Work and Economic Growth	No
9	Increase Industry, Innovation, and Infrastructure	Yes
10	Reduce Inequality	No
11	Mobilize Sustainable Cities and Communities	No
12	Influence Responsible Consumption and Production	No
13	Organize Climate Action	No
14	Develop Life Below Water	No
15	Advance Life On Land	No
16	Guarantee Peace, Justice, and Strong Institutions	No
17	Build Partnerships for the Goals	No

Justification

This research contributes to the Aviation and defense sector

Technical / Manufacturing Readiness Level

Select the Domain / Sector (Choose one (or) more appropriate option from the dropdown)

Sl No	Domain Description	Yes/No
1	Agriculture & Rural Development innovations	No
2	Consumer Goods and Retail/Supply Chain/ Logistics	No
3	Defence & Security	Yes
4	Food Processing / Biotech	No
5	Healthcare & Biomedical devices	No
6	Cyber-physical systems, Blockchain, AI & ML Applications	No
7	Industry 4.0	No
8	IoT based technologies	No
9	Manufacturing (Additive Manufacturing, 3D printing, etc.)	No
10	Hydrogen and other alternative fuel technologies.	No
11	New / Innovative Metals and Materials	No
12	Other Emerging Areas Innovation for Start-up	No
13	Product Design, Development and Management	Yes
14	Renewable and Affordable Energy	No
15	Robotics and Drones	No
16	Smart Education	No
17	Smart Vehicles/ Electric vehicle/ Electric vehicle motor and battery technology	No
18	Sustainable Environment	No
19	Waste Management/Waste to Wealth Creation	No
20	Circular economy and zero waste technologies	No

Justification

This research has significance in the field of Gas Turbine Engine Technology

Select the Innovation Type

Sl No	Innovation Type	Yes/No
1	Product	No
2	Process	Yes
3	Service	No
4	Market Place	No
5	Business/Management	No

Justification

A process to enhance turbine blade cooling has been formulated

Select the Technical Readiness Level (Choose one (or) more appropriate option from the dropdown)

Sl No	Readiness Level	Yes/No
1	Basic research, Principles postulated observed but no experimental proof available	Yes
2	Technology formulation. The concept and application have been formulated	Yes
3	Applied research. First laboratory tests completed; proof of concept	Yes
4	Small-scale prototype built in a laboratory environment (ugly prototype)	No
5	Large-scale prototype tested in the intended environment	No
6	Prototype system tested in an intended environment close to expected performance	No
7	Demonstration system operating in the operational environment at a pre-commercial scale	No
8	First-of-a-kind commercial system. Manufacturing issues solved	No
9	Full commercial application, the technology available for consumers	No

Justification

Proof of concept has been formulated

Select the Manufacturing Readiness Level (Choose one (or) more appropriate option from the dropdown)

Sl No	Readiness Level	Yes/No
1	Basic manufacturing implications identified	Yes
2	Manufacturing concepts identified	No
3	Manufacturing proof of concept developed	No
4	Capability to produce the technology in a laboratory environment	No
5	Capability to produce prototype components in a production-relevant environment	No
6	Capability to produce a prototype system or subsystem in a production-relevant environment	No
7	Capability to produce systems, subsystems, or components in a production-representative environment	No
8	Pilot line capability demonstrated. Ready to begin low-rate production.	No
9	Low rate production demonstrated. Capability in place to begin Full Rate Production.	No
10	Full rate production demonstrated and lean production practices in place	No

Justification

Additive manufacturing technology can be used to generate the proposed blade cooling configuration.

Course Outcome

Rating of Course Outcomes

CO No	Course Outcome	Rating
1	Formulate specific problem statements for ill-defined real-life problems with reasonable assumptions and constraints	5
2	Perform a literature search and/or patent search in the area of interest	4
3	Develop a suitable solution methodology for the problem	4
4	Conduct experiments / Design & Analysis/solution iterations and document the results	5
5	Perform error analysis/benchmarking / costing	5
6	Synthesise the results and arrive at scientific conclusions/products / solution	5
7	Document the results in the form of technical report/presentation	4